Creep Behaviour and Tensile Response of Adhesively Bonded Polyethylene Double-Strap Joints

M.A. Saeimi Sadigh [a], B. Paygozar [b,*], L.F.M. da Silva [c], E. Martínez-Pañeda [d]

[a] Department of Mechanical Engineering, Azarbaijan Shahid Madani University, Tabriz, Iran

[b] Department of Mechanical Engineering, TED University, Ankara, Turkey

[c] Department of Mechanical Engineering, Faculty of Engineering, University of Porto, Porto, Portugal

[d] Department of Civil and Environmental Engineering, Imperial College London, London SW7 2AZ, UK

[*] Corresponding: bahman.paygozar@tedu.edu.tr

Abstract: We investigate the static and time-dependent behaviour of adhesively bonded polyethylene Double-Strap (DS) joints to assess the feasibility of this mechanical bonding relative to Single-Lap (SL) joints. Both experiments and finite element simulations are conducted. First, we individually characterise the tensile and creep behaviour of the adhesive and adherent materials; Araldite and polyethylene, respectively. This information is used to develop suitable constitutive models that are then implemented in the commercial finite element package ABAQUS by means of user material subroutines. The numerical models are used to design the creep tests on the adhesive joints. Afterwards, an extensive experimental campaign is conducted where we characterise the static and creep behaviour of two joint configurations, SL and DS joints, and three selected values of the overlap length. In regards to the static case, the results reveal an increase in the failure load with increasing overlap length. Also, a slightly better performance is observed for the SL joint configuration. For the creep experiments, we show that the DS adhesive joint configuration leads to much shorter elongations, relative to

the SL joints. These differences diminish with increasing overlap length but remain substantial in all cases. In both joint configurations, the elongation increases with decreasing overlap length. Moreover, the numerical predictions show a good agreement with the experiments. The stress redistribution is investigated and it is found that the shear stress is highly sensitive to the testing time, with differences being more noticeable for the DS joint system.

Keywords: Creep behaviour; double-strap joint; single-lap joints; polyethylene.

1. Introduction

Adhesive joints are widely used across sectors due to their advantages relative to other competing joining technologies [1] [X]. Well-known advantages include weight reduction, fewer sources of stress concentration and reduced through-life maintenance [2] [X]. Adhesive joints can be classified into multiple groups according to their configuration; these include single-lap, double-lap, and scarf joints. In recent years, there has been an increasing interest in the repairment of adhesive joints, often using straps. This is motivated by applications exposed to potential sources of damage, especially in aeronautics, where other joining techniques such as riveting or bolting are not an option. As a consequence, a burgeoning literature has emerged with the aim of mitigating subsequent damage due to cracking (see, e.g. [3] [X] and references therein). This is often achieved by optimising the stress distribution. For example, by reducing the stiffness at the ends of the overlap, tapering the surface of the patches or using fillets filled with adhesives [4,5]. An alternative is to modify the stress distribution in the adhesive layers by means of the mixed modulus joint concept [6,7]. Also, embedded patches can be used to alter the stress distribution and augment the load transfer capacity of the joint [8,9]. Campilho *et al*. [10] investigated the tensile behaviour of adhesive single and Double-Straps joints with carbon-epoxy substrates. They found the optimal overlap length to be of 15 mm and the repair strength to be insensitive to

changes in patch thickness. However, when buckling load is considered the optimal overlap length changes and a sensitivity of repair strength to patch thickness is revealed [11]. Moreira and Campilho [12] investigated the use of scarf repairs in aluminium structures with and without reinforcement. They showed that, by using reinforcement, the sensitivity of the bonding strength to the scarf angle can be mitigated.

A promising material for joints adherents is polyethylene (PE). Widely used in a variety of sectors, polyethylene can favourably compete with metals due to its higher strength-to-weight ratio, bonding performance and resistivity against corrosion [13-16]. Studies have been conducted regarding the use of polyethylene adherents in lap-shear joints. Pinto *et al.* [17] measured the bonding strength of Single-Lap joints of adherents made of polyethylene, composite and aluminium. Barton and Birkett [18] assessed the tensile strength and impact behaviour of Single-Lap joints with PE adherents, considering the influence of surface preparation. Also in the context of Single-Lap joints, LeBono *et al.* [19] investigated the lap-shear strength performance of polyethylene pipeline bonded with acrylic adhesive in the temperature range -10 to +20 °C. They found that a decrease in curing/testing temperature to zero degrees resulted in a steady reduction in the lap-shear strength performance of the bonded joints. Very recently, Dehaghani *et al*. [20] assessed the influence of acid etching duration on the adhesive bonding strength of polyethylene on E-glass/epoxy composites. They found that both joint strength and fatigue resistance improved with increasing acid etching exposure time.

The response of adhesive joints under creep is of interest to many applications across the aerospace, transport, energy, and marine sectors [21] [X]. Accordingly, a number of experimental and numerical studies have been devoted to characterising the creep behaviour of adhesive joints. For instance, Dean [22] developed a model for non-linear creep in an epoxy adhesive under both dry and

humid conditions. Yu *et al.* [23] investigated the rate-dependent behaviour of epoxy-based adhesives using both power-law creep models and so-called unified theory models. Saeimi Sadigh *et al*. [24] combined experiments and modelling to characterise the creep behaviour of epoxy-based adhesive joints at different temperature levels. However, none of these studies deals with adhesively bonded polyethylene joints, motivating the present study. The creep behaviour of polyethylene has been a subject of interest outside of the adhesive joint community, see for example Refs. [25-28]. We build on this knowledge to characterise the behaviour of polyethylene-based adhesive joints.

In this work, we investigate for the first time the creep behaviour of adhesively bonded polyethylene strap joints. Both experiments and finite element simulations are conducted. First, the tensile and creep behaviour of the adherent and adhesive materials are characterised, experimentally and numerically. This information is then used to assess the performance of Single-Lap (SL) and Double-Strap (DS) joint configurations. Tensile tests are first conducted to characterise the mechanical response of the adhesive joints under monotonic loading. Creep tests are then performed to gain insight into the time-dependent response. In all cases, the role of the adherent length is explored by testing three different cases per adhesive joint configuration. In addition, finite element analysis is also conducted to gain further insight and assist in the interpretation of the results. The calibration of the numerical model enables conducting parametric studies, as needed for joint design across applications.

The paper is organised as follows. Section 2 presents the details of the experimental campaign. In Section 3, we describe the constitutive material models employed and the finite element framework developed. The numerical and experimental results are presented and discussed in Section 4. Finally, the manuscript conclusions are presented in Section 5.

2. Experimental study

We proceed to describe the testing procedures under tensile and uniaxial creep loading conditions. Tests were carried out on the adherent and adhesive materials, individually, and on both Single-Lap (SL) and double-strap (DS) joints. The outcome of the experimental campaign was used to inform the finite element model. The adherents of both the SL and DL joints were made of 5 mm thick high-density polyethylene (HDPE) sheets with dimensions 25x120 mm. These are bonded through a thin layer of epoxy-based structural adhesive, Araldite 2011. The mechanical properties of HDPE and the adhesive, as well as their time-dependent behaviour, are characterised by testing dog-bone samples manufactured following the ASTM D638 standard, as shown in Fig. 1b.

Two batches of SL and DS joints are manufactured with geometries and dimensions as given in Fig. 1c and 1d. Three different configurations were considered in each group, with characteristic overlap lengths of l_a=19 mm, 29 mm and 39 mm. Surface preparation of the adherents is carried out prior to the bonding process. Following the ASTM D 1780 standard recommendations, abrasive sandpaper is used to ensure a rough surface in the bonding domain of the joints. Subsequently, the adherents' surfaces were cleaned with acetone to remove contamination, followed by an etching process through H_2SO_4 solution. A special fixture described in Ref. [29] was used to ensure alignment of the adherents during the production process.

We examined first the tensile and creep behaviours of the adherent and adhesive materials. The uniaxial tension tests were conducted with a crosshead speed of 1.3 mm/min. While for the creep testing, we used constant loads at 65%, 75% and 85% of the material yield point (at room temperature). For this purpose, an automatic creep testing machine was employed to record the time-dependent displacement of the samples by means of an extensometer with 0.02 mm accuracy. The loading arm

of the machine adjusts the horizontal position automatically to ensure the application of a constant load during the test. The outcome of the tests was then used to inform the modelling of static and creep behaviour by means of suitable constitutive models.

Regarding the mechanical behaviour of the adhesive joints, both uniaxial tension tests and creep experiments were conducted. Tension tests are used to measure the load-displacement response and their maximum strength (Fig. 1a), relevant parameters in adhesive joint design. The loading rate corresponds to that used for the uniaxial tests on the adherent and the adhesive materials. Afterwards, creep tests were conducted to characterise the time-dependent behaviour of the joints. Creep tests of SL and DS joints were carried out at constant loads of 1.6 and 2 kN, and at a constant temperature of 25ºC.



(a)



(b)

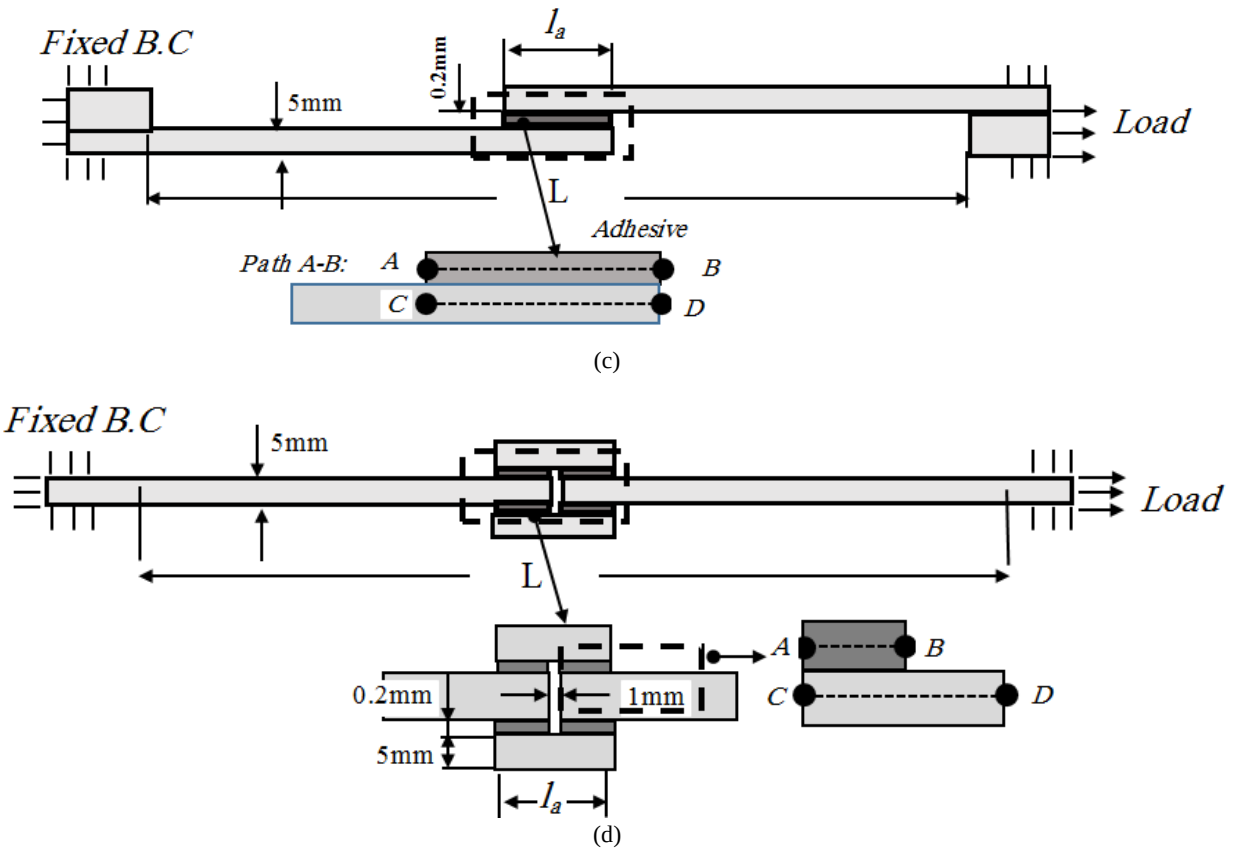


Fig. 1. Experimental equipment and sketches of the adhesive joint configurations: a) a single-lap joint under uniaxial tensile test, b) uniaxial creep test of a polyethylene bulk sample, c) single-lap (SL) joint, and d) double-strap (DS) joint.

3. Numerical model

In the following, we proceed to describe the constitutive models employed and the numerical framework that has been developed.

3.1 Constitutive models

The behaviour of the adherent and the adhesive is assumed to be elastic-plastic, in agreement with the tensile tests. J2 plasticity theory is used to model the adherent, as in [17] [X]. The hardening behaviour follows the uniaxial stress-strain response, see Section 4. On the other hand, the adhesive is pressure-sensitive and consequently the Drucker–Prager model is used to constitutively characterise its behaviour [30-32] [X]. Specifically, we adopt the general exponent form by which the yield function F is written in the meridional plane ($p-q$ plane) as:

$$F = aq^b - p - p_t = 0 \quad (1)$$

Where p_t is the hardening parameter that represents the hydrostatic tension strength of the material, and a and b are material parameters. For a given material yield stress in tension σ_Y and a hydrostatic-stress-sensitivity parameter λ, the values of a and p_t can be given as:

$$a = \frac{1}{\sigma_Y(\lambda - 1)} \quad (2)$$

$$p_t = a\lambda\sigma_Y^2 \quad (3)$$

Plastic flow is defined by the parameter ψ and is obtained from the following expression:

$$\tan\psi = \frac{3(1 - 2\nu^p)}{2(1 + \nu^p)} \quad (4)$$

where ν^p is the plastic component of Poisson's ratio [30] [X].

On the other hand, capturing the time-dependent behaviour of the adhesive joints requires modelling the creep behaviour of the adhesive, Araldite 2011, and the adherent, polyethylene. The experiments are conducted at a load level well below yielding, and accordingly the evolution of the creep strain as a function of time, $\varepsilon_c(t)$, is defined by subtracting the elastic strains to the total strains:

$$\varepsilon_c(t) = \varepsilon_{total}(t) - \varepsilon_{elastic} \quad (5)$$

The non-linear creep behaviour of polymers can be appropriately captured using a sufficient number of elastic and damping elements. Here, a model is used that combines spring and damper elements to derive the compliance equation of the material, as sketched in Fig. 2. This model is a combination of Zener and Maxwell models [33,34] and can capture both first and secondary creep stages. However,

attention is here limited to the response of adhesive joints in the primary creep regime.

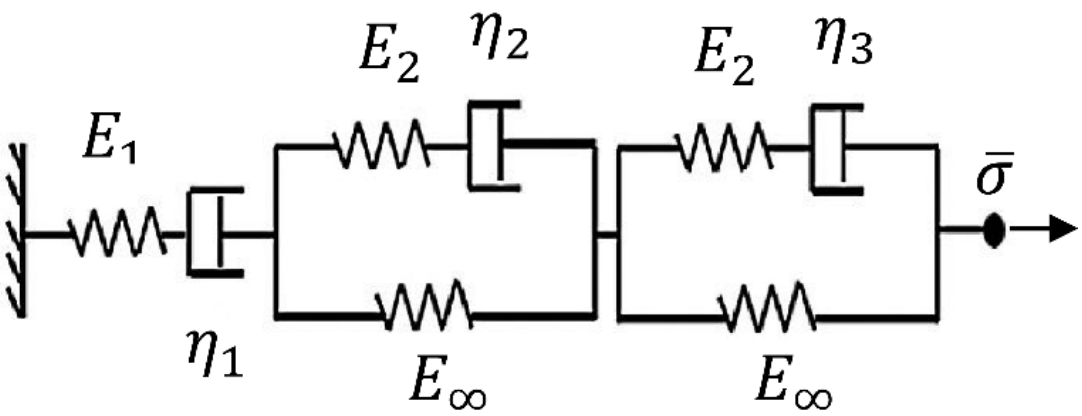


Fig. 2. Schematic representation of the combination of spring and damper elements used in the rheological model assumed, which is composed of one Maxwell and two Zener models.

The model compliance can be obtained by making use of Laplace's transform. For a given average stress σ_0, the evolution in time of the total strain is a function of several material constitutive parameters, as:

$$\varepsilon_{total}(t) = \sigma_0 \left[\frac{1}{E_1} + \frac{t}{\eta_1} + \frac{2}{E_\infty} - \frac{E_0 - E_\infty}{E_0} e^{-\frac{t}{\theta_1}} - \frac{E_0 - E_\infty}{E_0} e^{-\frac{t}{\theta_2}} \right] \tag{6}$$

The material parameters $(E_\infty, E_1, E_2, \eta_1, \eta_2)$ can be obtained through nonlinear regression on the experimental results of creep tests. On the other hand, the parameters E_0, θ_1 and θ_2 are defined as:

$$E_0 = E_\infty + E_2; \quad \theta_1 = \frac{\eta_2 E_0}{[E_\infty (E_0 - E_\infty)]}; \quad \theta_2 = \frac{\eta_3 E_0}{[E_\infty (E_0 - E_\infty)]} \tag{7}$$

Equation (6) can be reformulated [35] [X], such that the rheological model reads:

$$\varepsilon_{total}(t) = \varepsilon_e + \left[\alpha \hat{t} - \beta \left(e^{-a_5 \hat{t}} + e^{a_5 \hat{t}} \right) \right] = \varepsilon_e + \alpha \hat{t} + \beta \sinh(a_6 \hat{t}) \tag{8}$$

Where ε_e denotes the elastic strain and α and β are respectively referred to as the first and second-order functions of stress. The parameters α, β and $\hat{t}$ can be defined as follows:

$$\alpha = a_1 + a_2\sigma_0; \quad \beta = a_3 + a_4\sigma_0 + a_5\sigma_0^2 ; \quad \hat{t} = \log_{10}(t) \tag{9}$$

On the other hand, the parameters a_i are material constants that can be calculated from the experimental data by means of nonlinear regression techniques. In the present work, the mathematical software MATLAB is used to exact these coefficients – see Section 4.

3.2 Numerical implementation

The commercial finite element package ABAQUS is used to reproduce the experimental campaign described in Section 2. Geometric nonlinearity is accounted for. Three-dimensional models are developed to reproduce the SL and DS adhesive joint configurations shown in Figs. 1c and 1d. For the meshing, we use eight-node linear brick elements with reduced integration, C3D8R in ABAQUS notation. After a sensitivity analysis, it is found that numerical convergence is achieved when using about 16000 and 2400 elements in, respectively, the adherent and the adhesive parts. The boundary conditions employed mimic the experiments, as depicted in Figs. 1c and 1d. The same models are used for both the tensile and the creep tests. The constitutive model for creep behaviour described in Section 4.1 is implemented by means of a user material (UMAT) subroutine in ABAQUS.

4. Results and discussion

In this section, we describe the experimental and numerical results obtained, as well as their implications on adhesive joint behaviour and design. Tensile testing on the adherent and adhesive materials is described first, Section 4.1, followed by

their creep response, Section 4.2. In Section 4.3, we address the tensile response of the adhesive joints predicted both experimentally and numerically. Then, in Section 4.4, we examine the creep response of SL and DL adhesive joints and use the finite element model to gain further insight.

4.1 Tensile tests of the adherent and adhesive materials

Uniaxial tensile tests are conducted to characterise the mechanical response of the adherent, polyethylene, and the epoxy-based adhesive, Araldite 2011. The mechanical properties of polyethylene and the epoxy-based adhesive Araldite 2011 are listed in Table 1.

Table 1: Mechanical properties of polyethylene and the epoxy-based adhesive Araldite 2011.

	Araldite 2011	Polyethylene
Young's modulus, E (MPa)	1802 ± 20.1	1154 ± 15.4
Poisson's ratio, υ	0.29 ± 0.04	0.3 ± 0.2
Tensile yield strength, σ_y (MPa)	18 ± 0.6	14.02 ± 0.3
Tensile failure strength, σ_f (MPa)	26.36 ± 0.48	20.01 ± 0.25

A representative stress-strain curve for polyethylene is shown in Fig. 3. This stress-strain hardening behaviour is provided as input to the finite element model. Recall that J2 plasticity theory is used for polyethylene while the exponential form of Drucker-Prager is employed for the adhesive. The Drucker-Prager parameters used for Araldite 2011 are $a = 0.092$, $b = 2$ and dilatation angle $\psi = 13^{\circ}$.

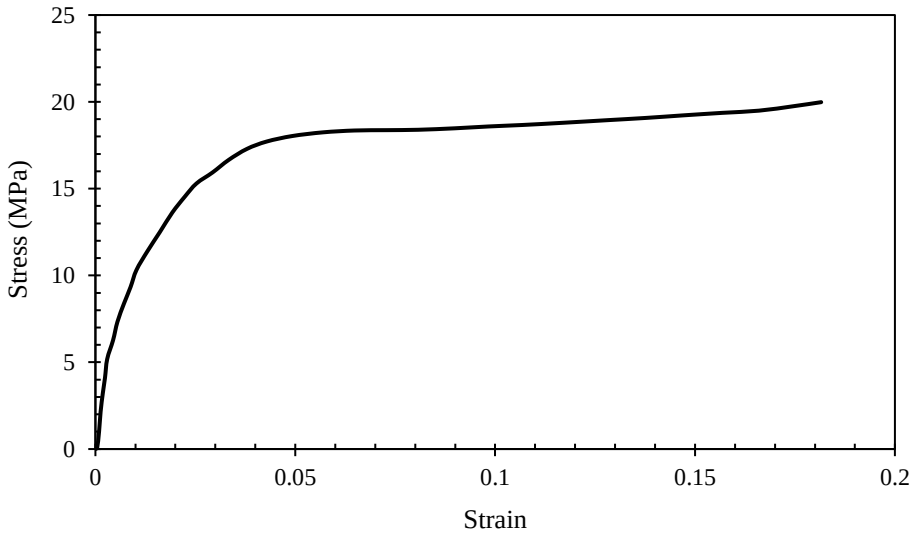


Fig. 3. The uniaxial stress-strain curve obtained from testing polyethylene.

4.2 Creep tests of the adherent and adhesive materials

We proceed to characterise the creep behaviour of the adhesive material, Araldite 2011, and the adherent material, polyethylene. The experiments are conducted under constant load and uniaxial tension conditions. Results obtained for the adhesive material are reported in Fig. 4, in terms of creep strain versus time (in

hours). Four selected values of the remote stress are considered: 15.3 MPa, 13.5 MPa, 11.7 MPa and 9.9 MPa. In agreement with expectations, the creep strain increases with the applied stress.

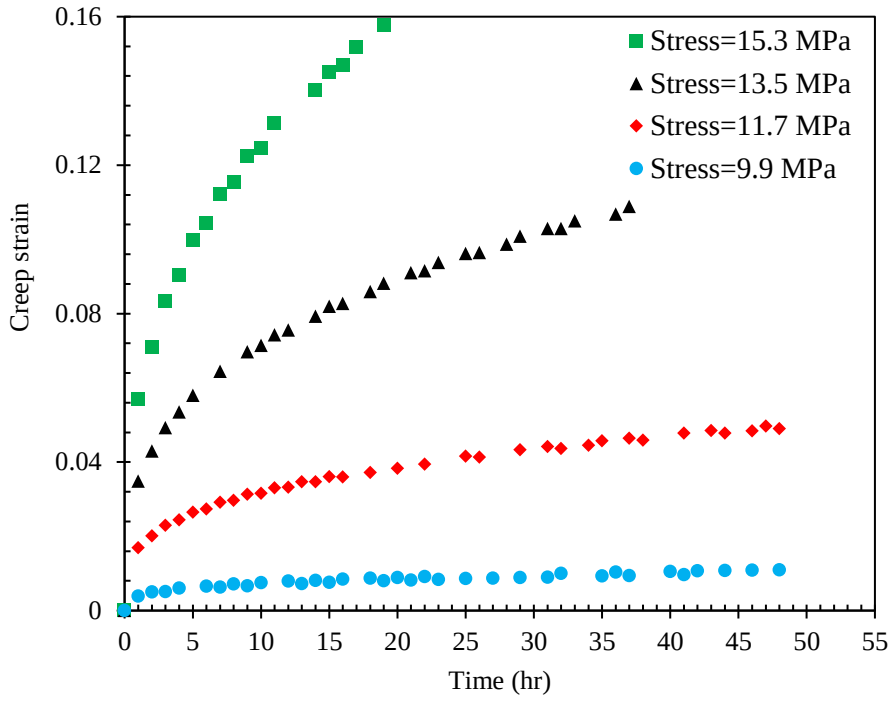


Fig. 4. Uniaxial creep test results for the adhesive material, Araldite 2011.

The results obtained for the adherent material, polyethylene, are shown in Fig. 5. Four remote load levels are considered, as characterised by remote stresses of 12 MPa, 10.5 MPa, 9 MPa and 7.5 MPa. As for the adhesive, the creep strain naturally increases with the applied stress. It is observed that the creep strain appears to saturate after approximately 200 hours.

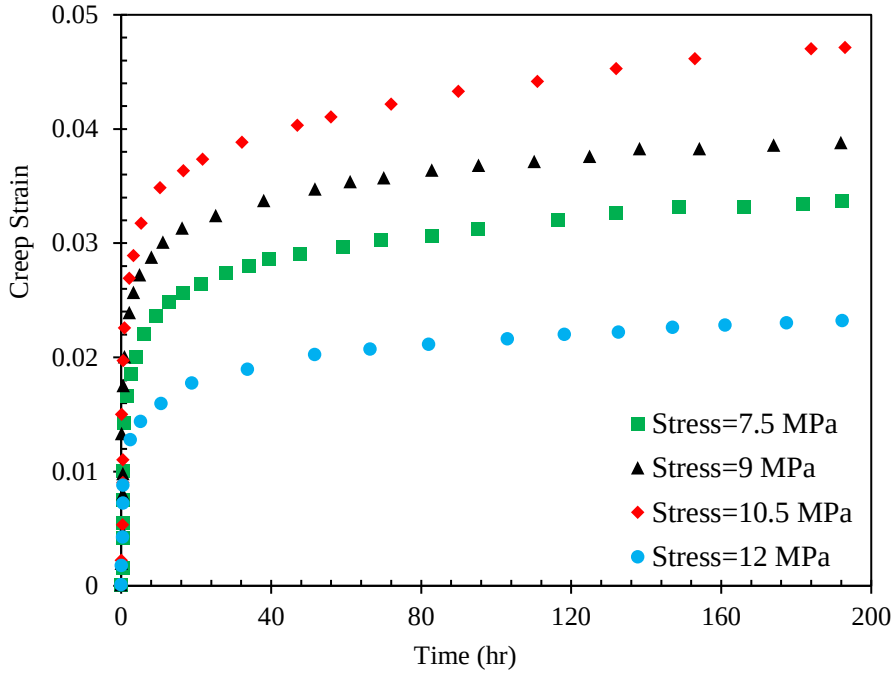


Fig. 5. Uniaxial creep test results for the adherent material, polyethylene.

The experimental data shown in Figs. 4 and 5 are used to calibrate the creep constitutive model outlined in Section 3.1. The software MATLAB is used to obtain the corresponding coefficients using nonlinear regression. For both the adhesive and adherent materials the coefficient of determination R^2 is very close to 1. The parameters obtained are listed in Table 3. The data was then used to model the creep behaviour of the adhesive joint systems.

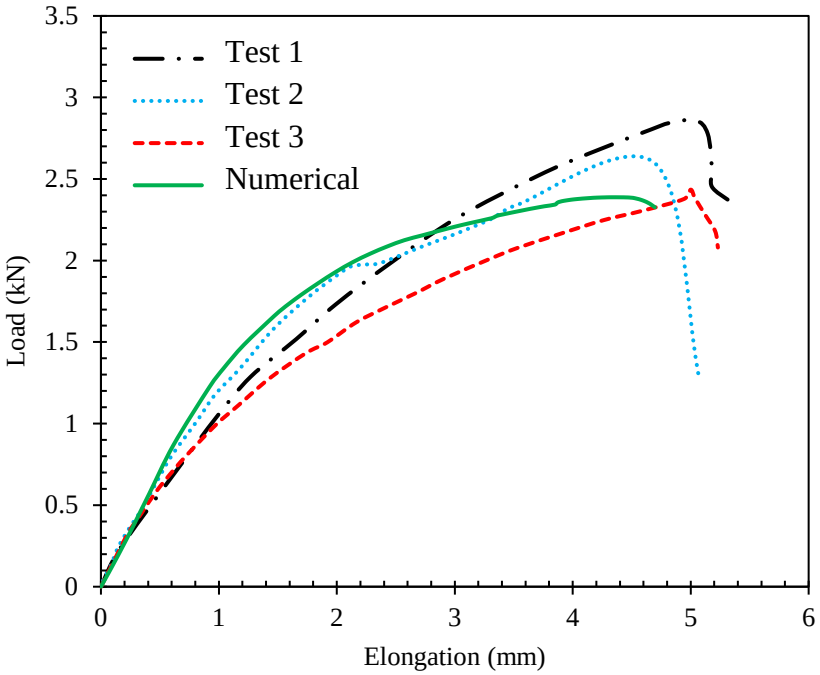
Table 3: Coefficients of creep constitutive model for the adhesive and the adherent materials.

	a_1	a_2	a_3	a_4	a_5	a_6	R^2
Adhesive	1.592E-02	-1.41E-03	5.50E-03	-2.284E-03	2.28E-04	0.92	0.991
Polyethylene	-2.06E-02	2.99E-04	9.10E-02	1.41E-02	-5.02E-04	1.22E-01	0.989

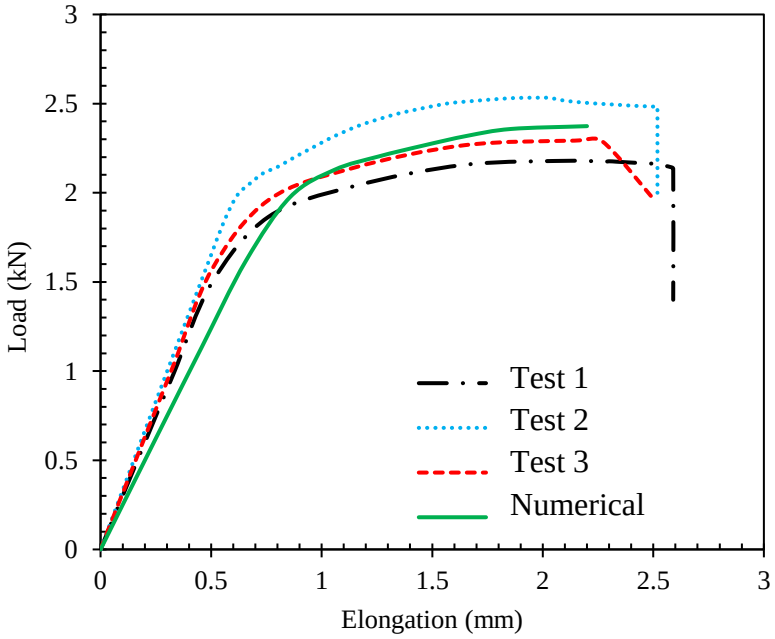
4.3 Modelling and testing of the tensile behaviour of adhesive joints

Once the individual constitutive behaviour of the adherent and the adhesive have been characterised, we proceed to model and test the behaviour of the single-lap (SL) and double-strap (DS) joints. The load versus displacement curves measured

from three sets of experiments are shown in Figs. 6a and 6b for, respectively, SL and DS joints. The case of an overlap length l_a=19 mm is considered. The three experiments conducted for each joint configuration show a good degree of reproducibility. In addition, the numerical prediction is also shown. The finite element results exhibit good agreement with the experiments in both the linear and non-linear regime, and for the two joint configurations considered.



(a)



(b)

Fig. 6. Load versus displacement curves obtained experimentally (3 tests) and numerically for adhesive joints with overlap length of l_a=19mm and subjected to uniaxial tension; a) Single-Lap (SL) adhesive joints, and b) Double-Strap (DS) adhesive joints.

Uniaxial tests were also conducted on SL and DS joints with overlap lengths of l_a=29 and 39 mm. The results obtained, in terms of the failure load, are shown in Fig. 7. We find that the failure loads are sensitive to the overlap length, with larger overlap lengths leading to higher failure loads. Also, SL joints appear to show a better performance, failing at higher load levels, relative to DS joints.

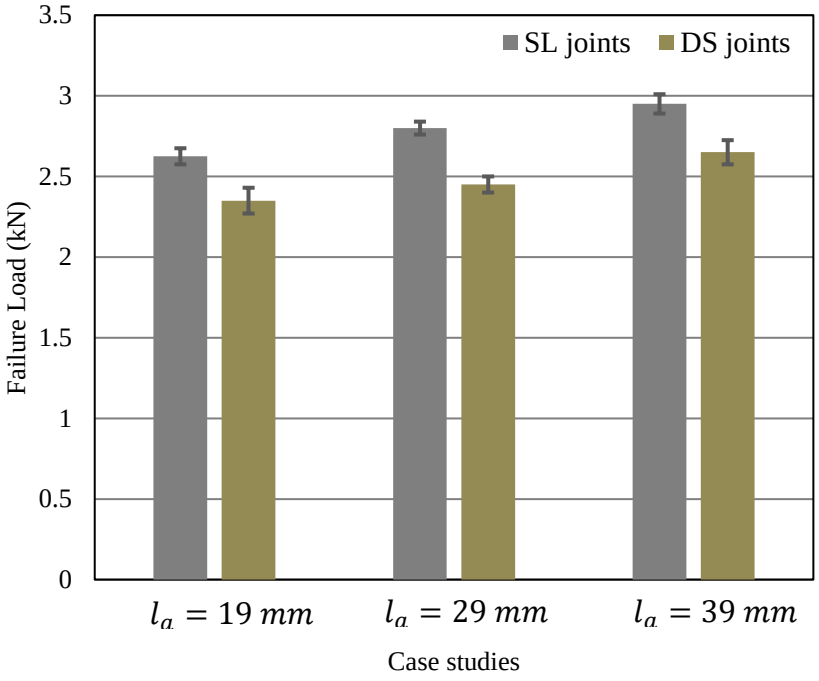


Fig. 7. Failure loads reported for Single-Lap (SL) and Double-Strap (DS) adhesive joint configurations and different overlap lengths l_a.

Once validated, the numerical model is employed to assist in the design of the creep experiments. The goal is to ensure that the applied load is sufficiently low such that no yielding occurs in the adhesive and, to a certain extent, in the adherent. First, the von Mises equivalent stress is plotted along the centre line of the adhesive, path A-B in Figs. 1c and 1d. The results are shown in Fig. 8 for a remote load of 2 kN and both SL and DS joints with different overlap lengths. The effective von Mises stress is shown normalised by the material yield stress and the distance along the centre line is normalised by the overlap length. It can be seen that a load of 2 kN is the highest that can be considered without triggering yielding

close to the edges of the adhesive. A similar trend is observed for the stress distribution in both SL and DS joints and, in all cases, smaller overlap lengths lead to higher stress values.

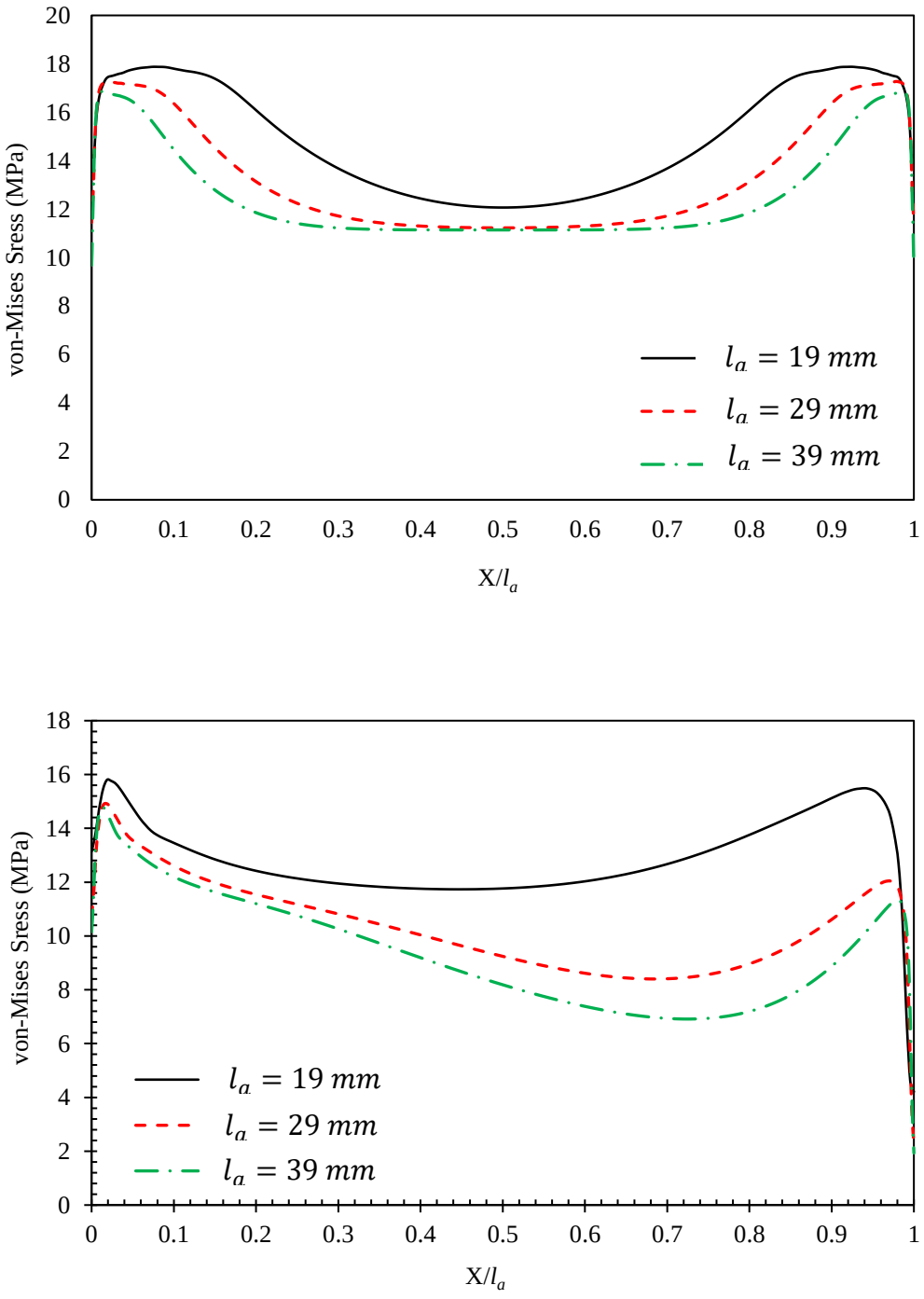


Fig. 8. Distribution of the von Mises effective stress along the centre line of the adhesive; (a) Single-Lap (SL) joint and (b) Double-Strap joint. The y axis indicates the ratio between the von Mises effective stress and the material yield stress, while the x axis shows the distance along the

AB path normalised by the overlap length l_a.

Secondly, the effective von Mises stress is also computed in the adherent material. The contours of equivalent von Mises stress are plotted in Fig. 9 for both SL and DS joint configurations; the units are MPa. The case of overlap length l_a=19 mm and remote load equal to 2 kN is chosen as representative. While the effective stress exceeds the yield stress in some small regions, it remains below overall and particularly underneath the overlap region.

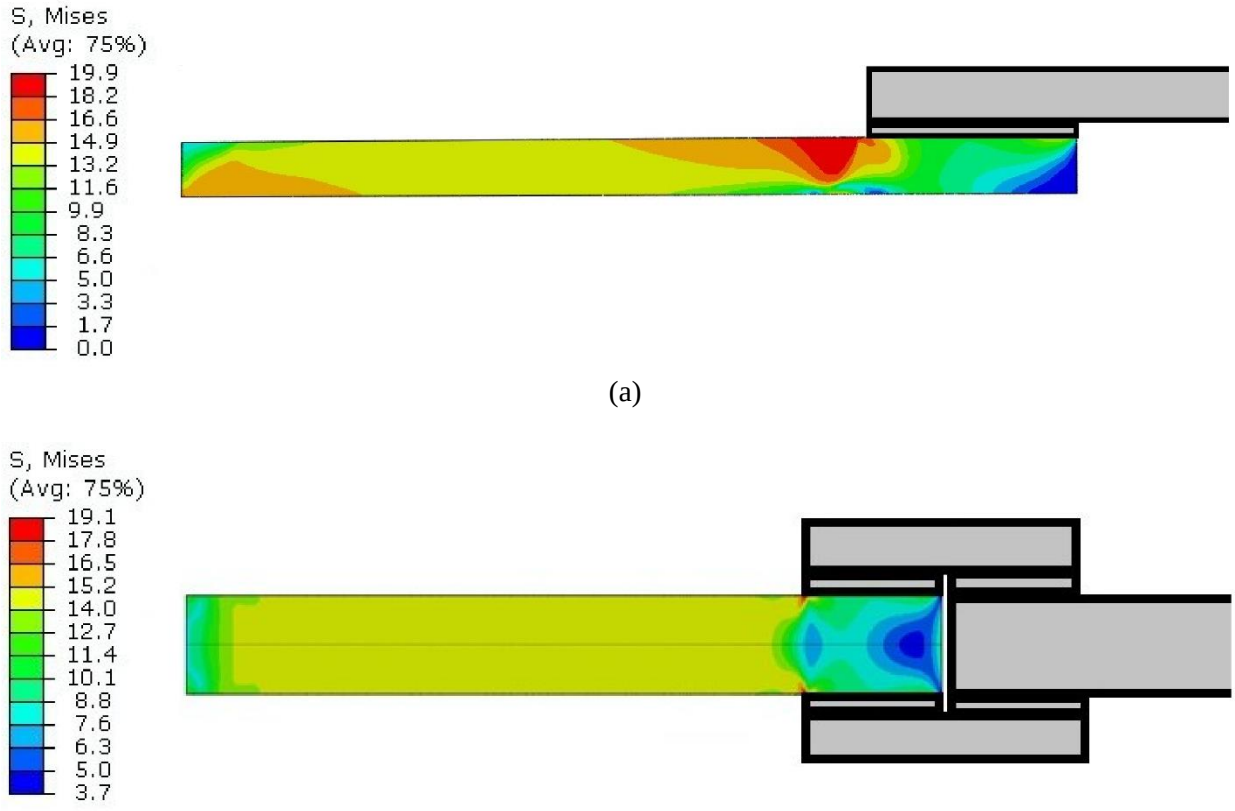
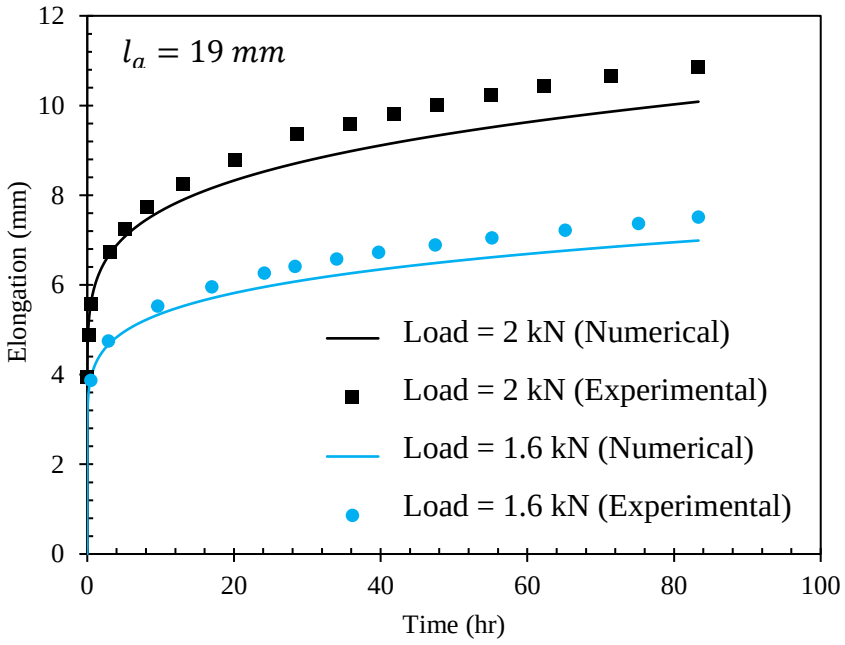


Fig. 9. Contours of von Mises stress (MPa) in the adherend material; (a) Single-Lap (SL) and (b) Double-Strap (DS) joint configurations.

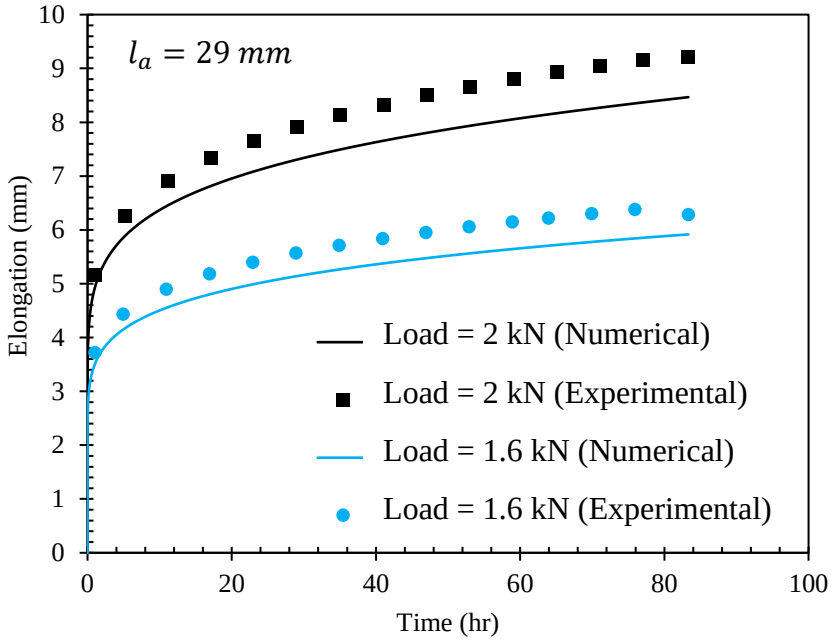
4.4 Modelling and testing of the creep behaviour of adhesive joints

Uniaxial creep tests are conducted on the adhesive joints following the results obtained in Section 5.3. Two adhesive joint configurations are considered, Single-

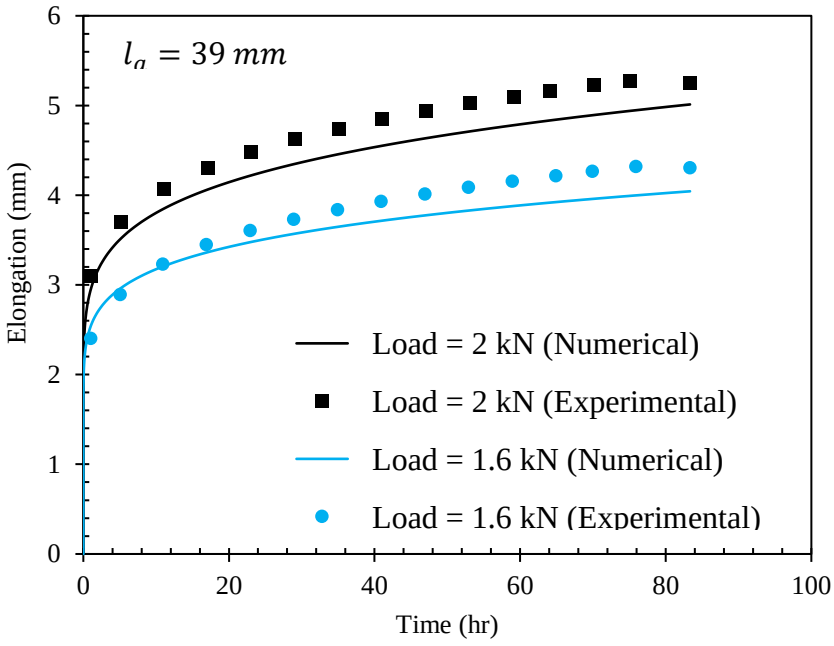
Lap (SL) and Double-Strap (DS) and, for each configuration, we vary the overlap length l_a, as for the uniaxial monotonic tests. Six adhesive joint configurations are considered, and each of them is subjected to two remote loads: 1.6 and 2 kN; a total of 12 case studies. The experiments are conducted for 83 hours to characterise the primary creep regime. None of the samples fails during this time. The results obtained for each case study are shown in Fig. 10 in terms of the elongation versus the testing time. In addition, the numerical predictions obtained with the model presented in Section 4, and calibrated as described above, are also shown. Symbols denote experimental results while solid lines are used to describe the finite element predictions. The numerical results slightly underpredict the experimental elongation-time responses but the agreement is satisfactory.



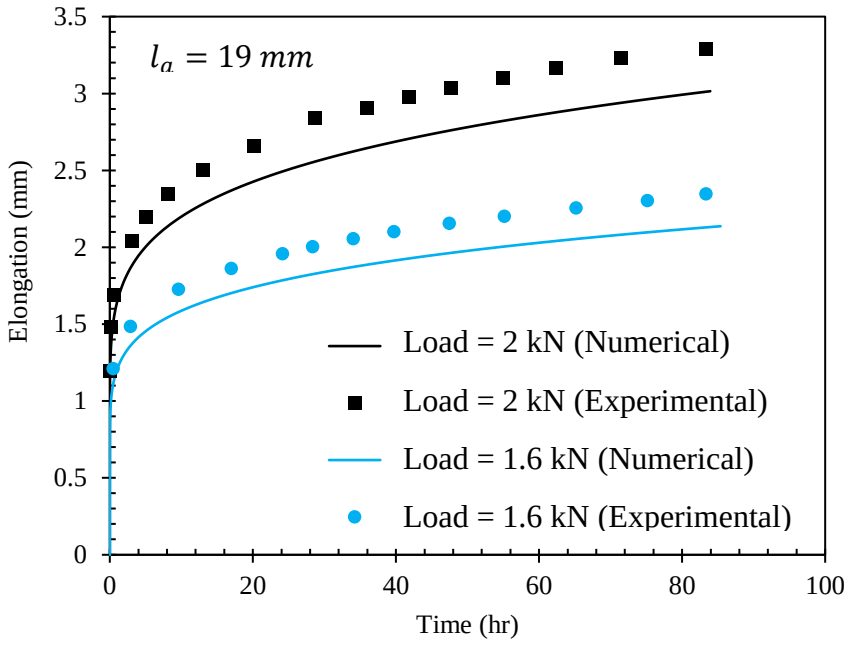
(a)


$l_a = 29\ mm$
Elongation (mm)
Time (hr)
Load = 2 kN (Numerical)
Load = 2 kN (Experimental)
Load = 1.6 kN (Numerical)
Load = 1.6 kN (Experimental)

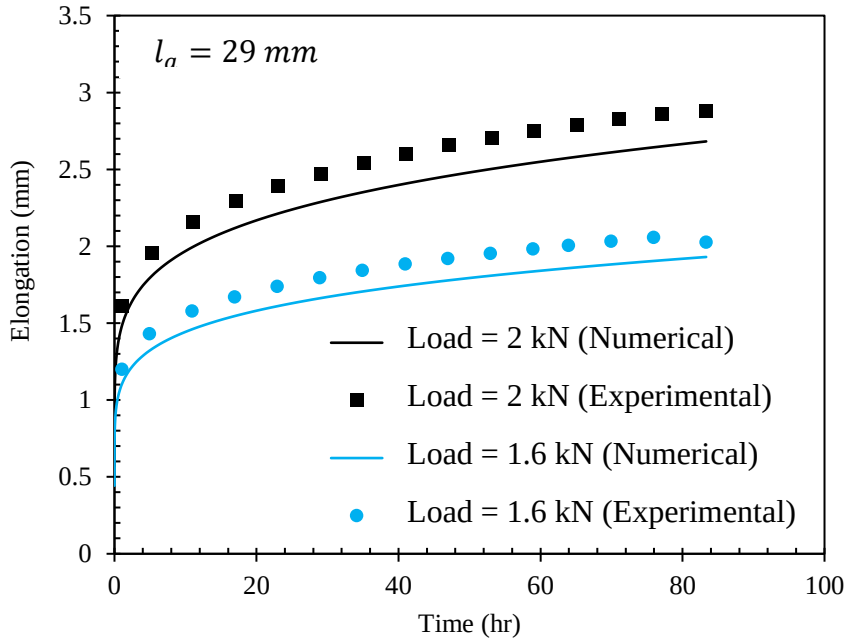
(b)


$l_a = 39\ mm$
Elongation (mm)
Time (hr)
Load = 2 kN (Numerical)
Load = 2 kN (Experimental)
Load = 1.6 kN (Numerical)
Load = 1.6 kN (Experimental)

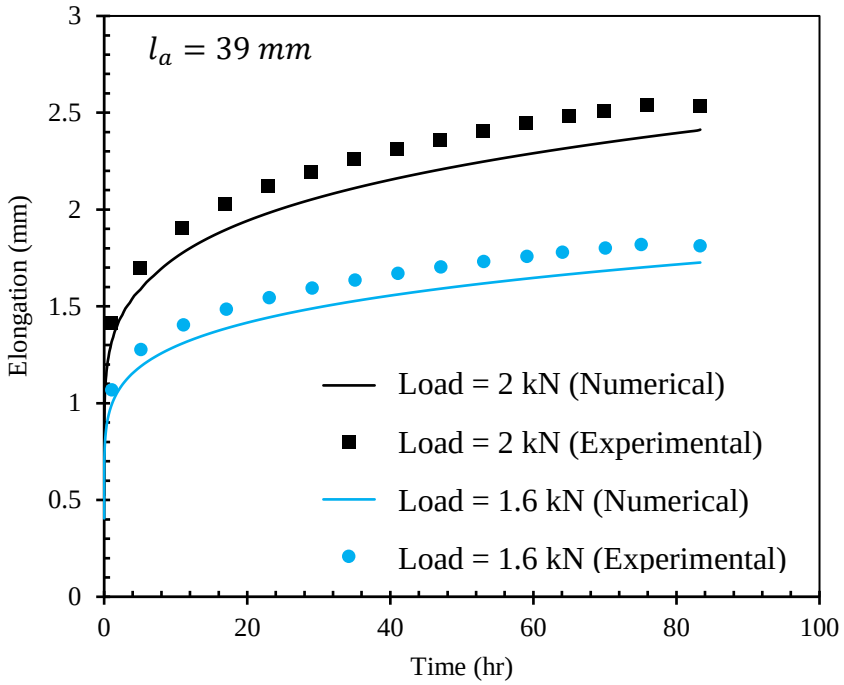
(c)


$l_a = 19\ mm$
Elongation (mm)
Time (hr)
Load = 2 kN (Numerical)
Load = 2 kN (Experimental)
Load = 1.6 kN (Numerical)
Load = 1.6 kN (Experimental)
0
0.5
1
1.5
2
2.5
3
3.5
0
20
40
60
80
100

(d)


$l_a = 29\ mm$
Elongation (mm)
Time (hr)
Load = 2 kN (Numerical)
Load = 2 kN (Experimental)
Load = 1.6 kN (Numerical)
Load = 1.6 kN (Experimental)
0
0.5
1
1.5
2
2.5
3
3.5
0
20
40
60
80
100

(e)



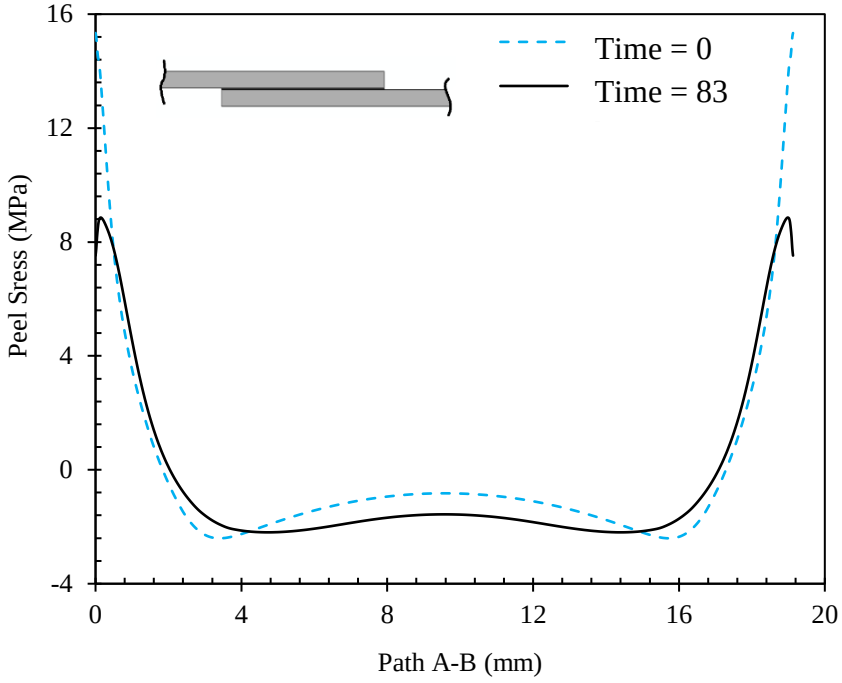
(f)

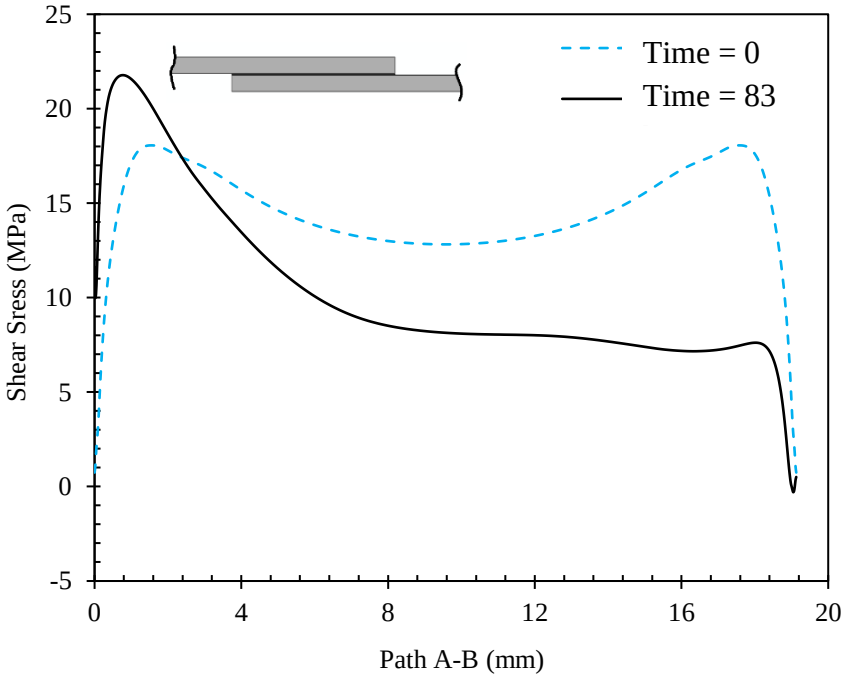
Fig. 10. Experimental and numerical time-elongation responses under creep loading of Single-Lap (SL) joints (a): l_a=19 mm (b): l_a=29 mm (c): l_a=39 mm and Double-Strap (DS) joints (d): l_a=19 mm (e): l_a=29 mm (f): l_a=39 mm.

In both the experimental and numerical predictions, the following trends can be observed. First, in both SL and DS joints, the elongation increases with decreasing the overlap length. Also, in agreement with expectations, the elongation increases with the applied load. Thirdly, significantly higher elongations are observed in the Single-Lap joints, relative to the Double-Strap configuration. For example, for l_a=19 mm and a load of 2 kN, the maximum elongation recorded for the SL joints is larger than three times the DS measurement; 10 mm and 3 mm, respectively. These differences increase with diminishing overlap length but remain substantial in all cases; for an overlap length of l_a=39 mm the elongation of SL joints is approximately twice of that predicted by DS joints for the same remote load.

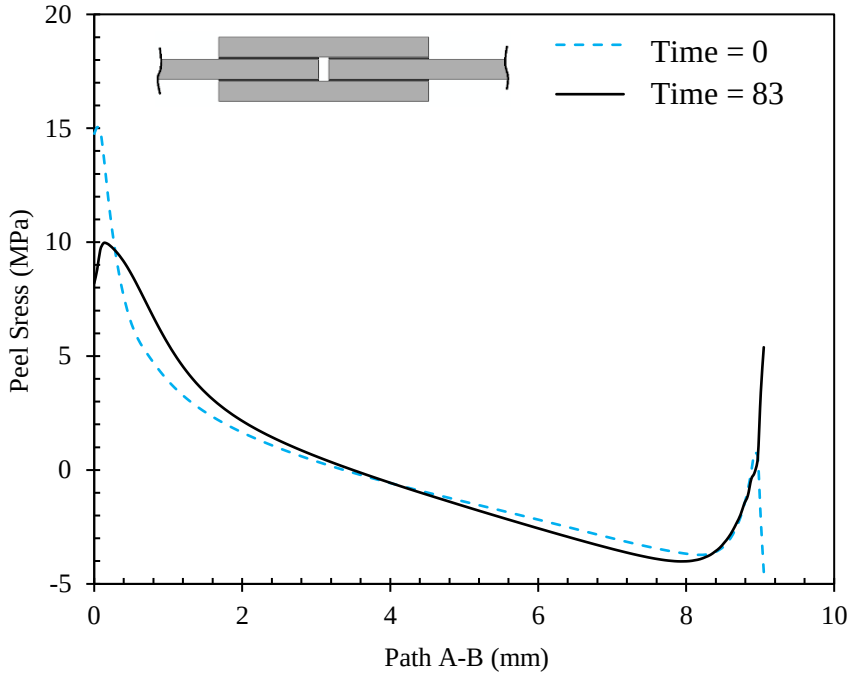
We proceed to gain further insight into the creep response by making use of the numerical model. Specifically, we aim at quantifying the stress redistribution that occurs during the testing. First, we compute the peel and shear stresses along the centre line of the adhesive, referred to as path A-B in Figs. 1c and 1d. The stress

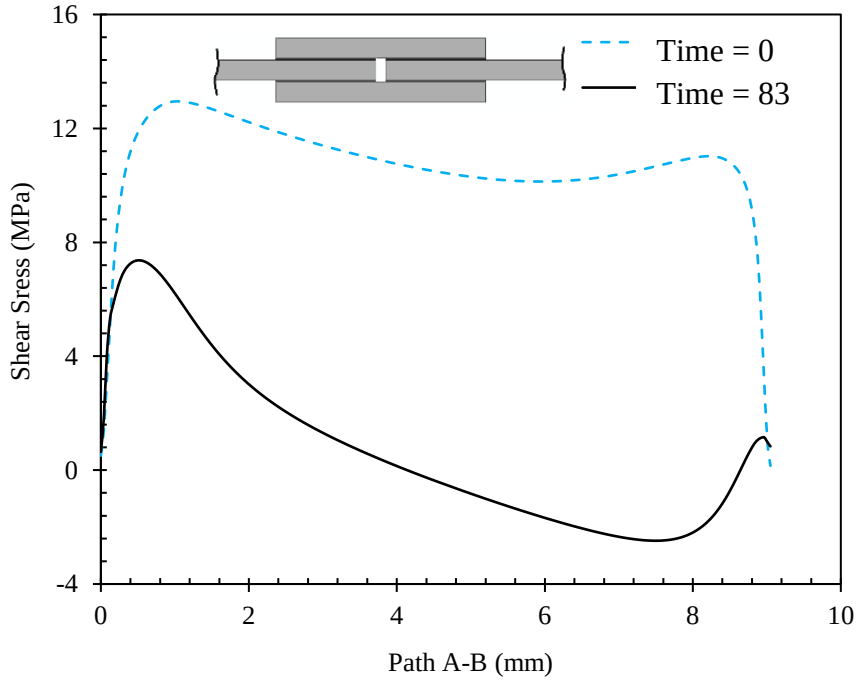
distributions are calculated at the end of the loading step ($t \approx 0$) and the end of the creep test ($t = 83$ h). The results are shown in Fig. 11 for the representative case of an overlap length $l_a = 19\,mm$, and for both SL and DS adhesive joint configurations.





(a)



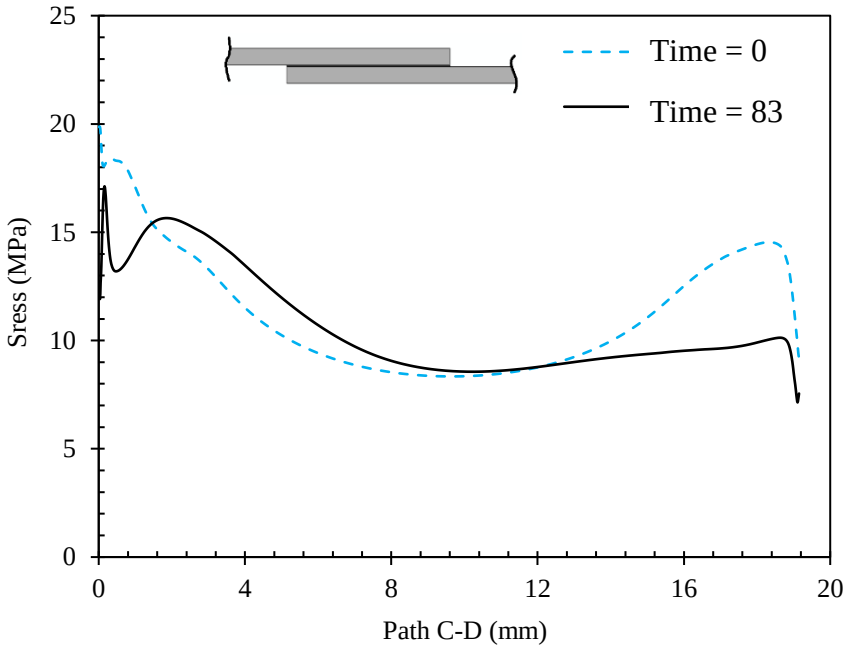


(b)

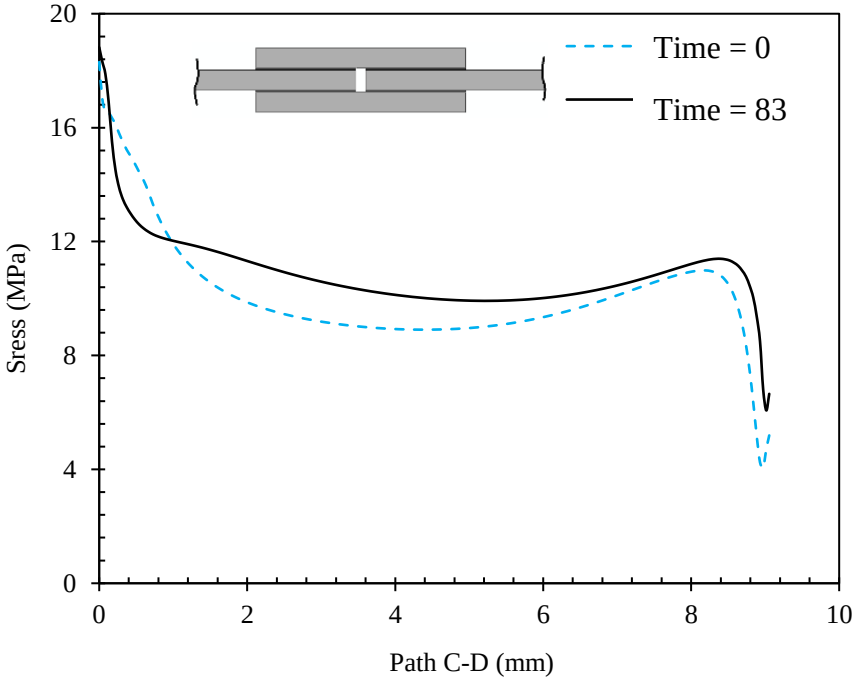
Fig. 11. Stress redistribution along the centre-line of the adhesive, path A-B. The result at the end of the loading step ($t \approx 0$) is given by a dashed line, while the result at the end of the creep test ($t \approx 83$ h) is given by a solid line. (a) Single-Lap (SL), and (b) Double-Strap (DS) joints. The case of overlap length $l_a = 19\ mm$ is taken as reference.

The results reveal that the peel stress is almost insensitive to creep loading. However, substantial changes are observed in the shear. In both SL and DS joints the shear stress level decreases with the testing time at almost every point of the adhesive layer. The drop is particularly significant in the case of the Double-Strap joint configuration, where negative shear stresses are attained in a region of the path.

We also explore the stress state in the adherent, see Fig. 12. The effective von Mises stress is plotted along the centre line of the adherent, polyethylene, at both the end of the loading step ($t \approx 0$) and the end of the creep test ($t = 83$ h). Again, both Single-Lap (SL), Fig. 12a, and Double-Strap (DS), Fig. 12b configurations are considered. Overall, a small stress redistribution is observed. In this case, differences with the initial state are more noticeable for the Single-Lap configuration, with relevant stress changes being observed at the edge of the path.



(a)



(b)

Fig.12 Stress redistribution along the centre-line of the adherent, path C-D. The result at the end of the loading step ($t \approx 0$) is given by a dashed line, while the result at the end of the creep test ($t \approx 83$ h) is given by a solid line. (a) Single-Lap (SL), and (b) Double-Strap (DS) joints. The case of overlap length $l_a = 19\ mm$ is taken as reference.

5. Conclusion

We investigated, numerically and experimentally, the static and creep behaviour of polyethylene-based Single-Lap (SL) and Double-Strap (DS) adhesive joints. First, insight is gained into the behaviour of the adherent and adhesive bulk materials, and a suitable rheological model is developed to capture their time-dependent response. The model is implemented in the finite element package ABAQUS by programming a user material subroutine. A large experimental campaign is conducted to evaluate the behaviour of SL and DS joints under static and time-dependent conditions for different load levels and overlap lengths. By combining experiments and numerical simulations we reveal the following findings:

- SL joints slightly outperform DS joints under uniaxial tension. In both systems, the failure load increases with the overlap length.

- Under creep conditions and for a given remote load, SL joints reveal much larger elongations than DS joints. Differences decrease with increasing overlap length but remain substantial in all cases.

- Little redistribution of the peel stress is observed in the adhesive. However, the shear stress shows a notable sensitivity to the testing time, and this effect is more pronounced for the DS joint configuration.

The numerical model shows a very good agreement with the experiments, strengthening the constitutive choices and enabling the assessment of multiple configurations for optimising adhesive joint design.

References:

1. P. Camanho, S.R. Hallett, Composite Joints and Connections: Principles, Modelling and Testing, Elsevier Science, 2011
2. L.F.M. da Silva, A. Öchsner, R.D. Adams, Handbook of Adhesion Technology, Springer Berlin Heidelberg, 2011
3. E. Martínez-Pañeda, I.I. Cuesta, N.A. Fleck, Mode II Fracture of an Elastic-Plastic Sandwich Layer, *Journal of Applied Mechanics*, **87**(3), (2019)
4. E.A.S. Marques, L.F.M. da Silva, Joint Strength Optimization of Adhesively Bonded Patches, *The Journal of Adhesion*, **84**(11), 915-934 (2008)
5. M. Sandu, A. Sandu, D.M. Constantinescu, D.A. Apostol, Single-strap adhesively bonded joints with square or tapered adherends in tensile test conditions, *International Journal of Adhesion and Adhesives*, **44**, 105-114 (2013)
6. B. Bachir Bouiadjra, H. Fekirini, M. Belhouari, B. Boutabout, B. Serier, Fracture energy for repaired cracks with bonded composite patch having two adhesive bands in aircraft structures, *Computational Materials Science*, **40**(1), 20-26 (2007)
7. Ş. Temiz, Application of bi-adhesive in double-strap joints subjected to bending moment, *Journal of Adhesion Science and Technology*, **20**(14), 1547-1560 (2006)
8. A. Pinto, R. Campilho, I.R. Mendes, A. Baptista, Strap repairs using embedded patches: Numerical analysis and experimental results, 2014
9. Ş. Çitil, Ş. Temiz, H. Altun, A. Özel, Determination of Mechanical Properties of Double-Strap Adhesive Joints with an Embedded Patch, *Journal of Adhesion Science and Technology*, **25**(18), 2555-2567 (2011)
10. R.D.S.G. Campilho, M.F.S.F. de Moura, D.A. Ramantani, J.J.L. Morais, J.J.M.S. Domingues, Tensile behaviour of three-dimensional carbon-epoxy adhesively bonded single- and double-strap repairs, *International Journal of Adhesion and Adhesives*, **29**(6), 678-686 (2009)
11. R.D.S.G. Campilho, M.F.S.F. de Moura, D.A. Ramantani, J.J.L. Morais, J.J.M.S. Domingues, Buckling strength of adhesively-bonded single and double-strap repairs on carbon-epoxy structures, *Composites Science and Technology*, **70**(2), 371-379 (2010)
12. R.D.F. Moreira, R.D.S.G. Campilho, Strength improvement of adhesively-bonded scarf repairs in aluminium structures with external reinforcements, *Engineering Structures*, **101**, 99-110 (2015)
13. E.M. Hoàng, D. Lowe, Lifetime prediction of a blue PE100 water pipe, *Polymer Degradation and Stability*, **93**(8), 1496-1503 (2008)
14. S. Bhowmik, T.K. Chaki, S. Ray, F. Hoffman, L. Dorn, Experimental investigation into the effect of DC glow discharge pretreatment of HDPE on tensile lap shear strength, *International Journal of Adhesion and Adhesives*, **24**(6), 461-470 (2004)
15. K. Navaneetha Pandiyaraj, V. Selvarajan, R.R. Deshmukh, C. Gao, Adhesive properties of polypropylene (PP) and polyethylene terephthalate (PET) film surfaces treated by DC glow discharge plasma, *Vacuum*, **83**(2), 332-339 (2008)
16. K. Leskovics, M. Kollár, P. Bárczy, A study of structure and mechanical properties of welded joints in polyethylene pipes, *Materials Science and Engineering: A*, **419**(1), 138-143 (2006)
17. A.M.G. Pinto, A.G. Magalhães, R.D.S.G. Campilho, M.F.S.F. de Moura, A.P.M. Baptista, Strength Prediction and Experimental Validation of Adhesive Joints Including Polyethylene, Carbon-Epoxy and Aluminium Adherends, *Materials Science Forum*, **636-637**, 1157-1164 (2010)

18. L. Barton, M. Birkett, Mechanical behaviour of adhesively bonded polyethylene tapping tees, *International Journal of Adhesion and Adhesives*, **66**, 1-8 (2016)
19. J. LeBono, L. Barton, M. Birkett, Low temperature tensile lap-shear testing of adhesively bonded polyethylene pipe, *International Journal of Adhesion and Adhesives*, **74**, 57-63 (2017)
20. R. Chitsaz Dehaghani, M.M. Shokrieh, F. Taheri-Behrooz, An investigation on effects of acid etching duration on adhesive bonding of polyethylene to E-glass/epoxy composites, *International Journal of Adhesion and Adhesives*, **85**, 177-183 (2018)
21. D. Dillard, Advances in Structural Adhesive Bonding, Elsevier Science, 2010
22. G. Dean, Modelling non-linear creep behaviour of an epoxy adhesive, *International Journal of Adhesion and Adhesives*, **27**(8), 636-646 (2007)
23. X.X. Yu, A.D. Crocombe, G. Richardson, Material modelling for rate-dependent adhesives, *International Journal of Adhesion and Adhesives*, **21**(3), 197-210 (2001)
24. M.A.S. Sadigh, B. Paygozar, L.F.M. da Silva, F.V. Tahami, Creep deformation simulation of adhesively bonded joints at different temperature levels using a modified power-law model, *Polymer Testing*, **79**, 106087 (2019)
25. R.K. Krishnaswamy, Analysis of ductile and brittle failures from creep rupture testing of high-density polyethylene (HDPE) pipes, *Polymer*, **46**(25), 11664-11672 (2005)
26. K.-h. Nitta, H. Maeda, Creep behavior of high density polyethylene under a constant true stress, *Polymer Testing*, **29**(1), 60-65 (2010)
27. H.B.H. Hamouda, M. Simoes-betbeder, F. Grillon, P. Blouet, N. Billon, R. Piques, Creep damage mechanisms in polyethylene gas pipes, *Polymer*, **42**(12), 5425-5437 (2001)
28. F. Vakili-Tahami, M.R. Adibeig, Using developed creep constitutive model for optimum design of HDPE pipes, *Polymer Testing*, **63**, 392-397 (2017)
29. M. Zehsaz, F. Vakili-Tahami, M.-A. Saeimi-Sadigh, Parametric study of the creep failure of double lap adhesively bonded joints, *Materials & Design*, **64**, 520-526 (2014)
30. G. Dean, L. Crocker, B. Read, L. Wright, Prediction of deformation and failure of rubber-toughened adhesive joints, *International Journal of Adhesion and Adhesives*, **24**(4), 295-306 (2004)
31. F.J. Guild, K.D. Potter, J. Heinrich, R.D. Adams, M.R. Winsom, Understanding and control of adhesive crack propagation in bonded joints between carbon fibre composite adherends II. Finite element analysis, *International Journal of Adhesion and Adhesives*, **21**(6), 445-453 (2001)
32. A.B. de Morais, A.B. Pereira, J.P. Teixeira, N.C. Cavaleiro, Strength of epoxy adhesive-bonded stainless-steel joints, *International Journal of Adhesion and Adhesives*, **27**(8), 679-686 (2007)
33. F. Mainardi, G. Spada, Creep, relaxation and viscosity properties for basic fractional models in rheology, *The European Physical Journal Special Topics*, **193**(1), 133-160 (2011)
34. W. Zhang, X. Guo, G. Kassab, A Generalized Maxwell Model for Creep Behavior of Artery Opening Angle, *Journal of biomechanical engineering*, **130**, 054502 (2008)
35. M. Zehsaz, F. Vakili-Tahami, M.A. Saeimi-Sadigh, Modified creep constitutive equation for an epoxy-based adhesive with nonlinear viscoelastic behavior, *The Journal of Strain Analysis for Engineering Design*, **50**, 4-14 (2015)

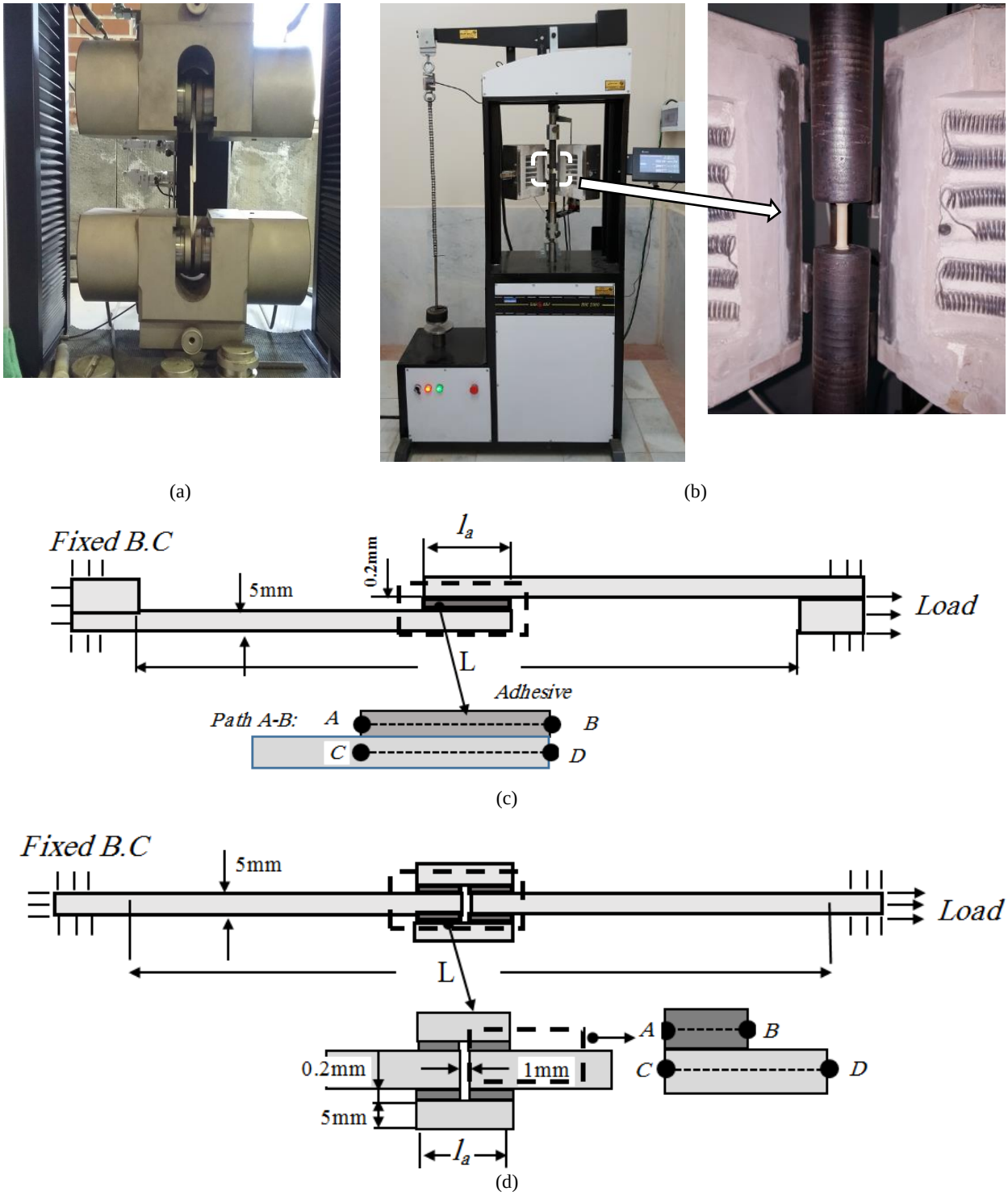


Fig. 1. Experimental equipment and sketches of the adhesive joint configurations: a) a single-lap joint under uniaxial tensile test, b) uniaxial creep test of a polyethylene bulk sample, c) single-lap (SL) joint, and d) double-strap (DS) joint.

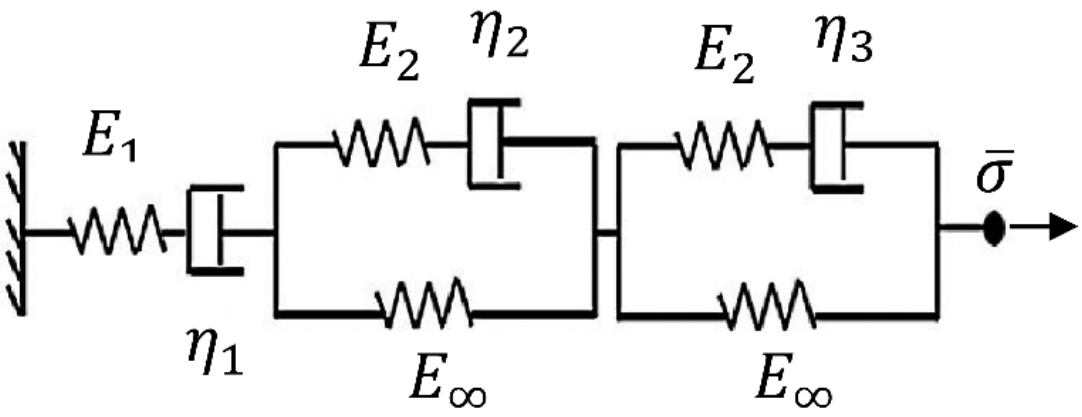


Fig. 2. Schematic representation of the combination of spring and damper elements used in the rheological model assumed, which is composed of one Maxwell and two Zener models.

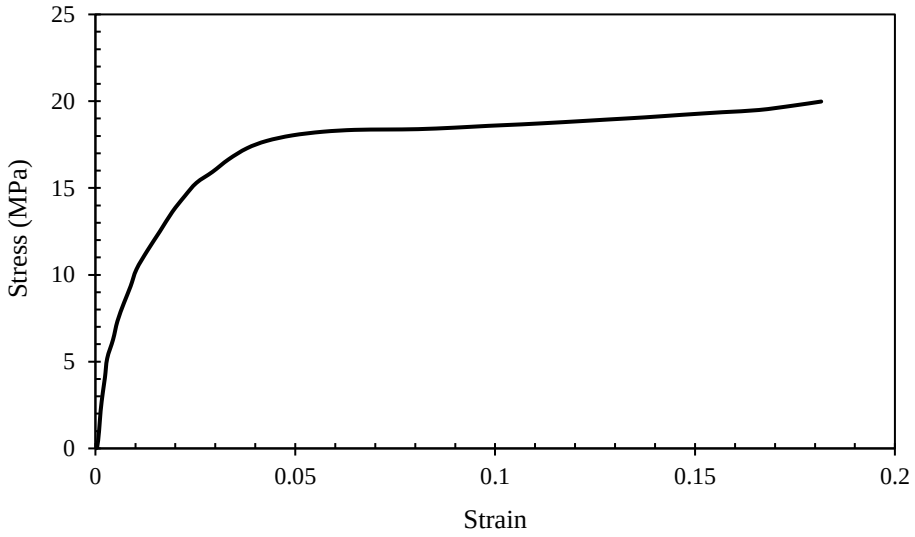


Fig. 3. Uniaxial stress-strain curve obtained from testing polyethylene.

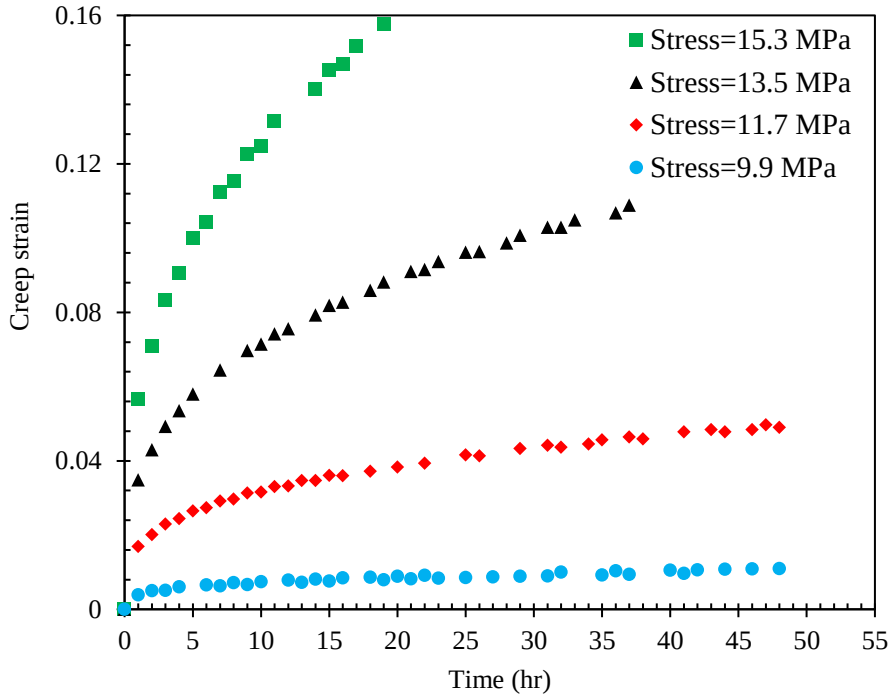


Fig. 4. Uniaxial creep test results for the adhesive material, Araldite 2011.

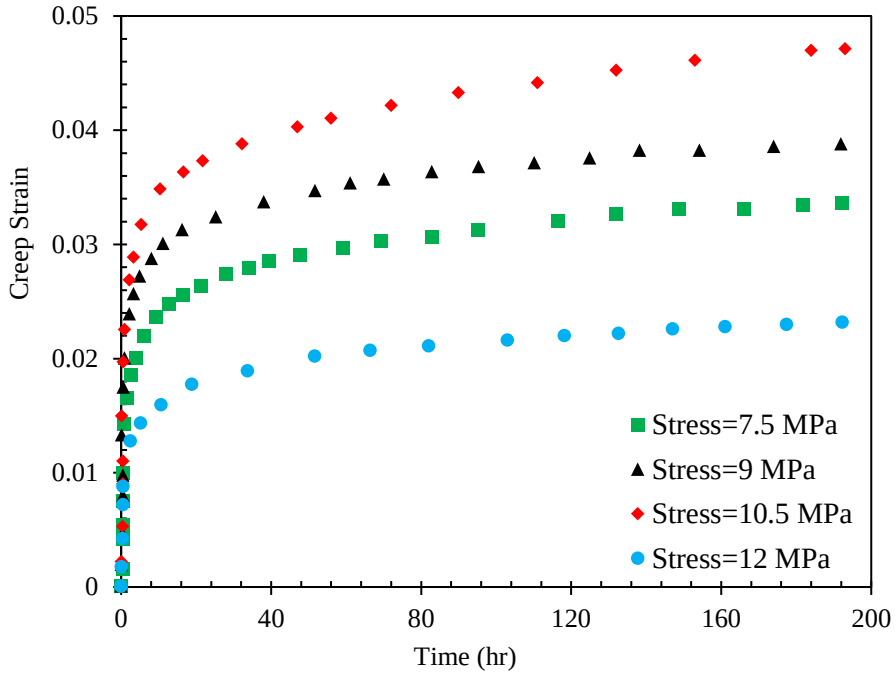
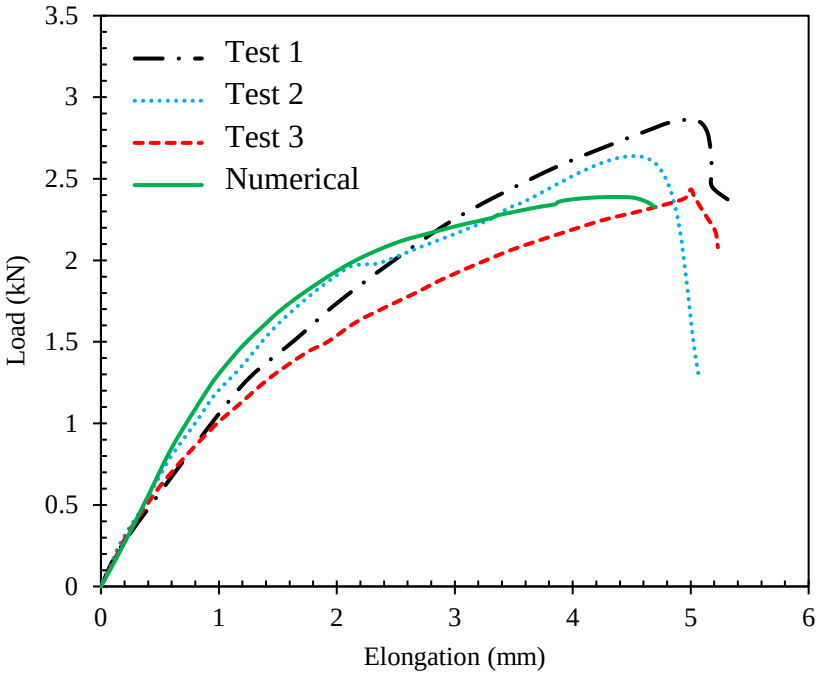
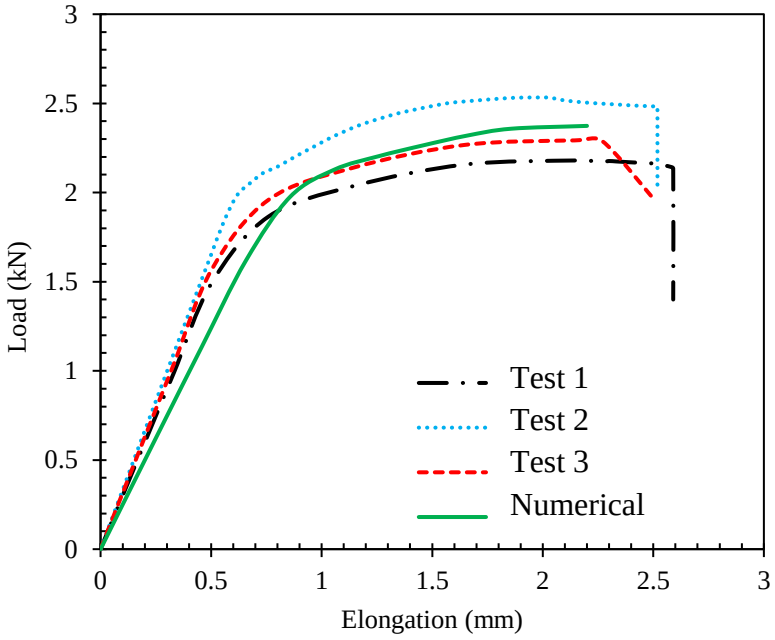


Fig. 5. Uniaxial creep test results for the adherent material, polyethylene.



(a)



(b)

Fig. 6. Load versus displacement curves obtained experimentally (3 tests) and numerically for adhesive joints with overlap length of l_a=19mm and subjected to uniaxial tension; a) Single-Lap (SL) adhesive joints, and b) Double-Strap (DS) adhesive joints.

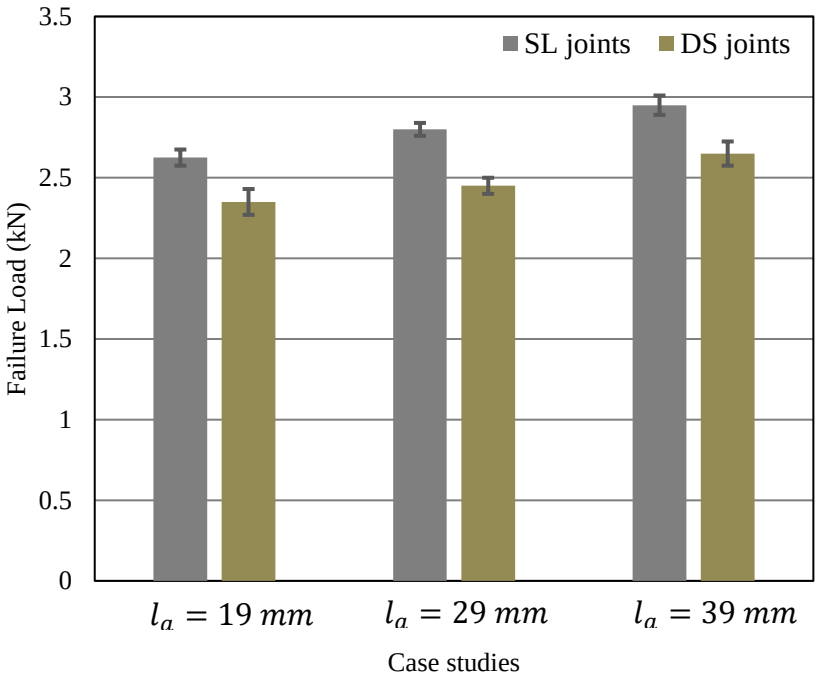
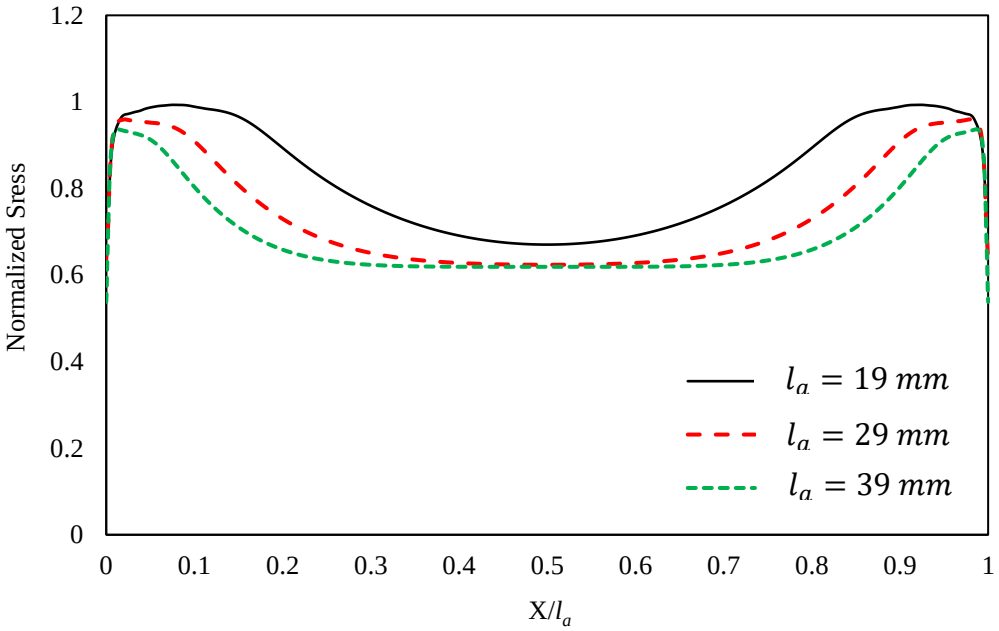


Fig. 7. Failure loads reported for Single-Lap (SL) and Double-Strap (DS) adhesive joint configurations and different overlap lengths l_a.



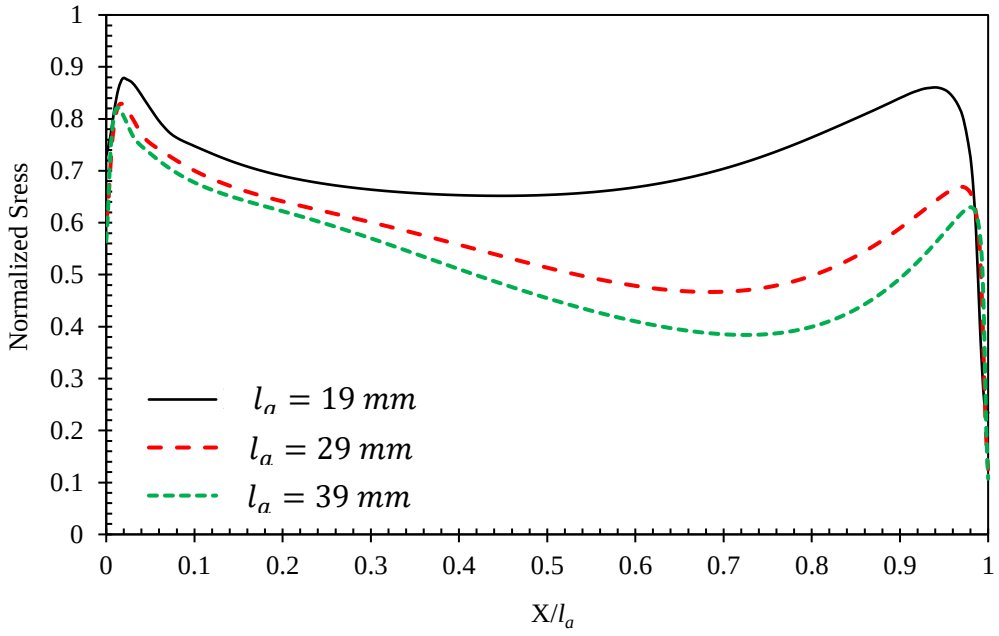
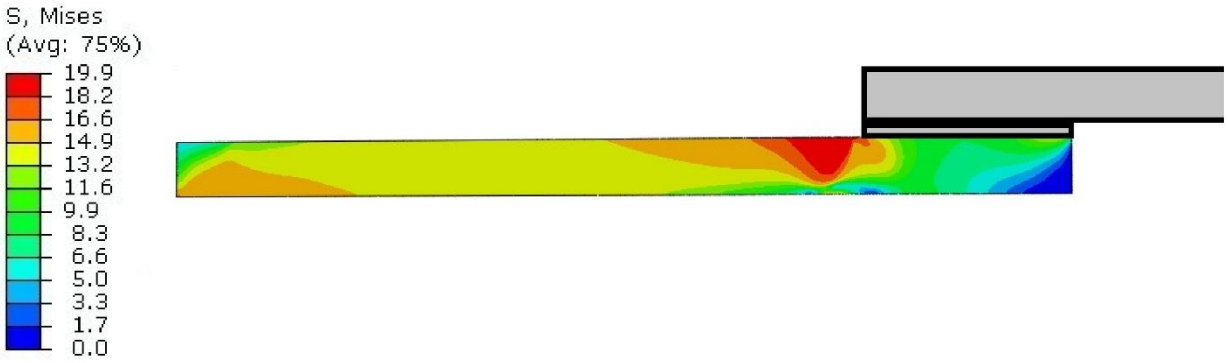
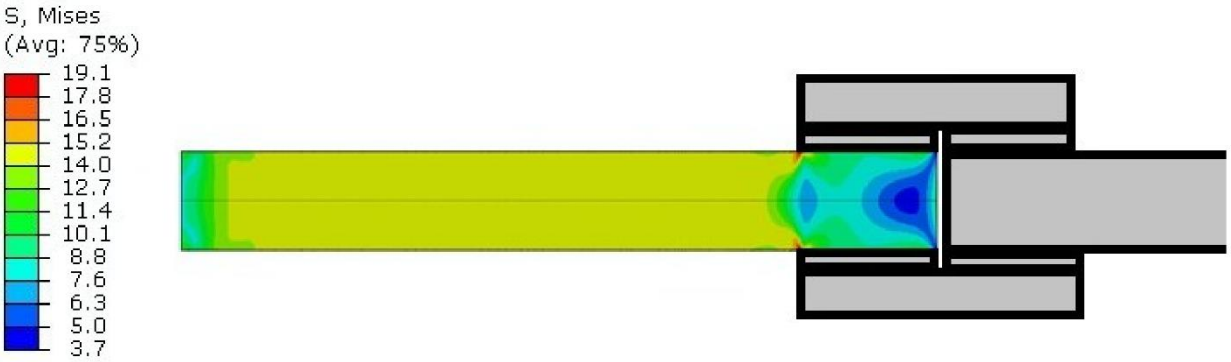


Fig. 8. Distribution of the von Mises effective stress along the centre line of the adhesive; (a) Single-Lap (SL) joint and (b) Double-Strap joint. The y axis indicates the ratio between the von Mises effective stress and the material yield stress, while the x axis shows the distance along the AB path normalised by the overlap length l_a.

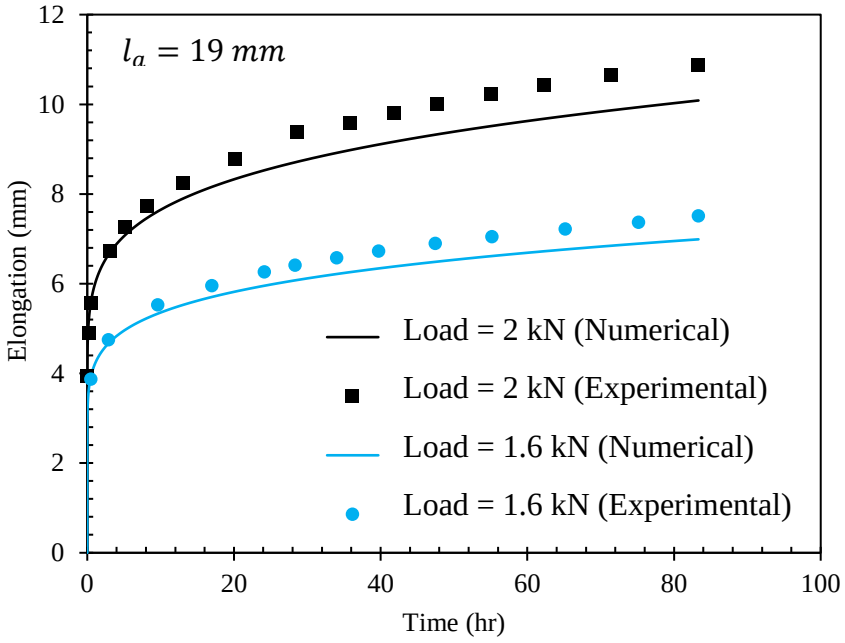


(a)

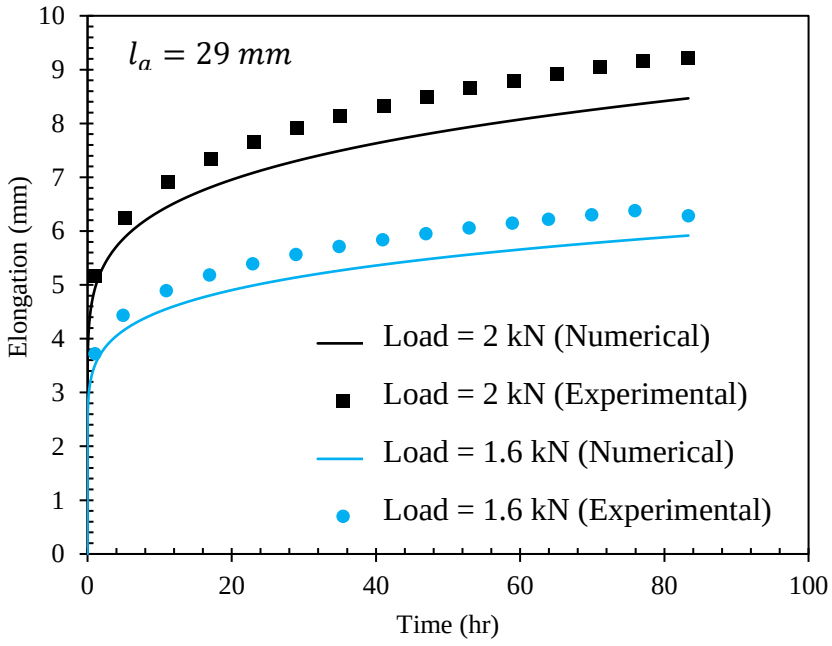


(b)

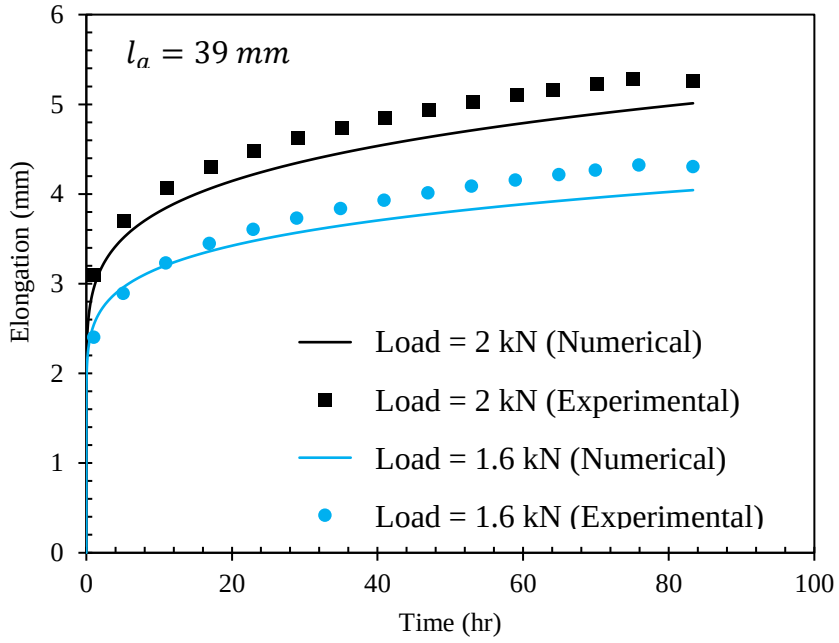
Fig. 9. Contours of von Mises stress (MPa) in the adherend material; (a) Single-Lap (SL) and (b) Double-Strap (DS) joint configurations.


$l_a = 19\ mm$
Elongation (mm)
Time (hr)
Load = 2 kN (Numerical)
Load = 2 kN (Experimental)
Load = 1.6 kN (Numerical)
Load = 1.6 kN (Experimental)

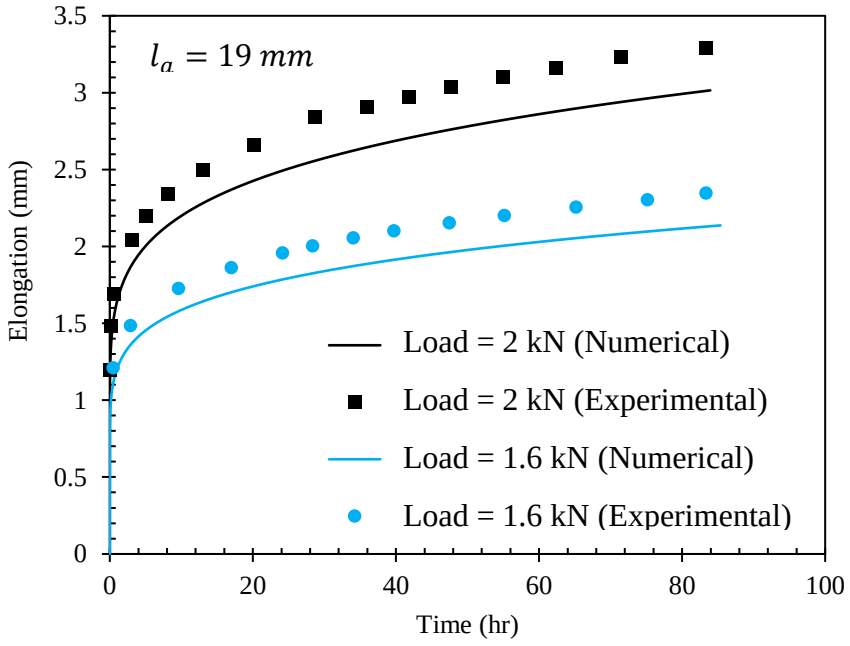
(a)


$l_a = 29\ mm$
Elongation (mm)
Time (hr)
Load = 2 kN (Numerical)
Load = 2 kN (Experimental)
Load = 1.6 kN (Numerical)
Load = 1.6 kN (Experimental)

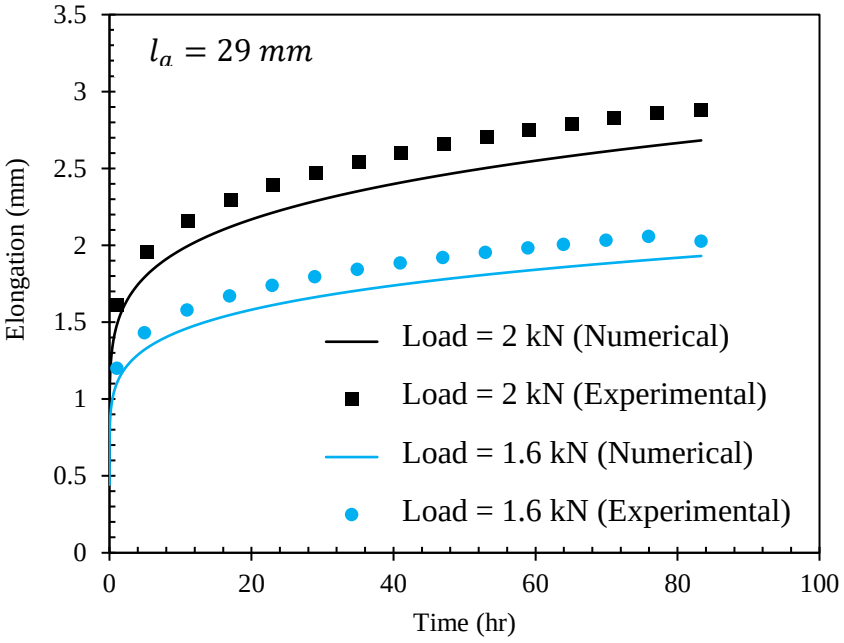
(b)


$l_a = 39\ mm$
Elongation (mm)
Time (hr)
Load = 2 kN (Numerical)
Load = 2 kN (Experimental)
Load = 1.6 kN (Numerical)
Load = 1.6 kN (Experimental)
0
1
2
3
4
5
6
0
20
40
60
80
100

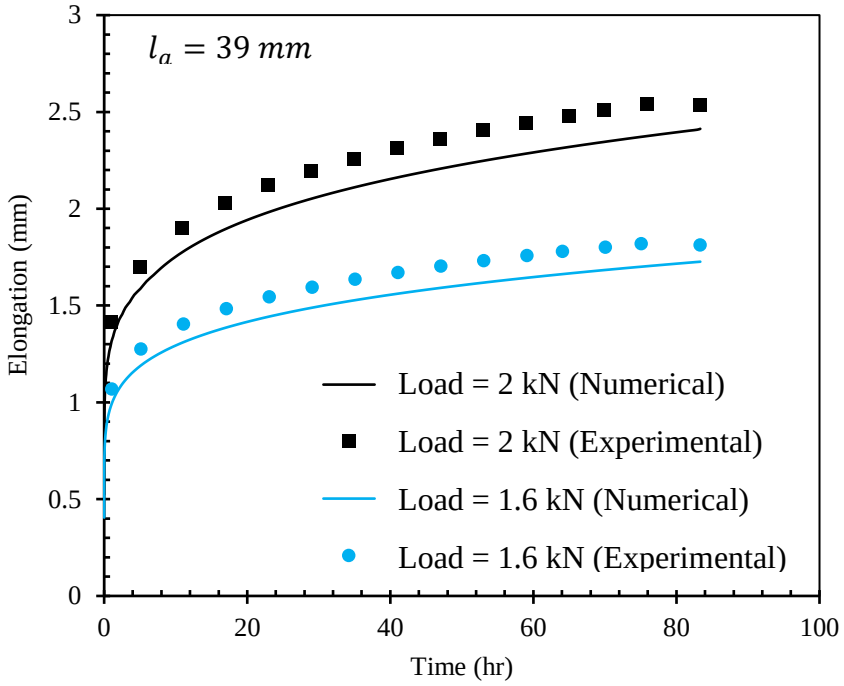
(c)


$l_a = 19\ mm$
Elongation (mm)
Time (hr)
Load = 2 kN (Numerical)
Load = 2 kN (Experimental)
Load = 1.6 kN (Numerical)
Load = 1.6 kN (Experimental)
0
0.5
1
1.5
2
2.5
3
3.5
0
20
40
60
80
100

(d)

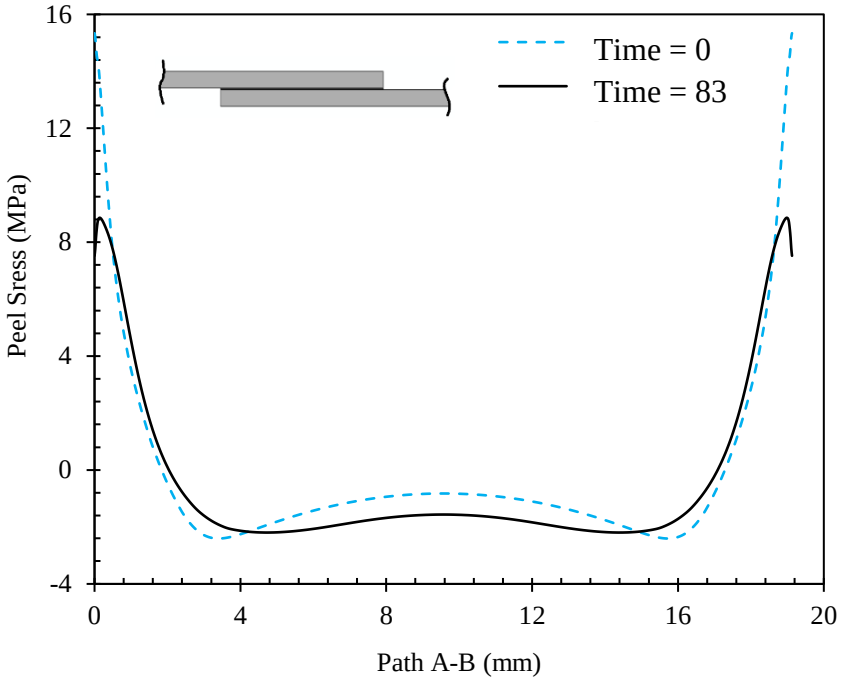


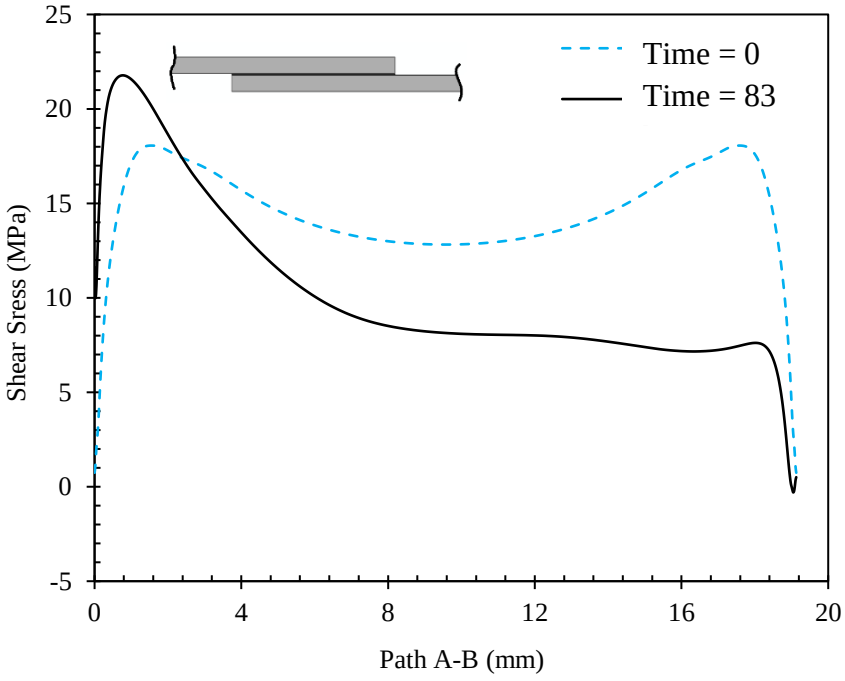
(e)



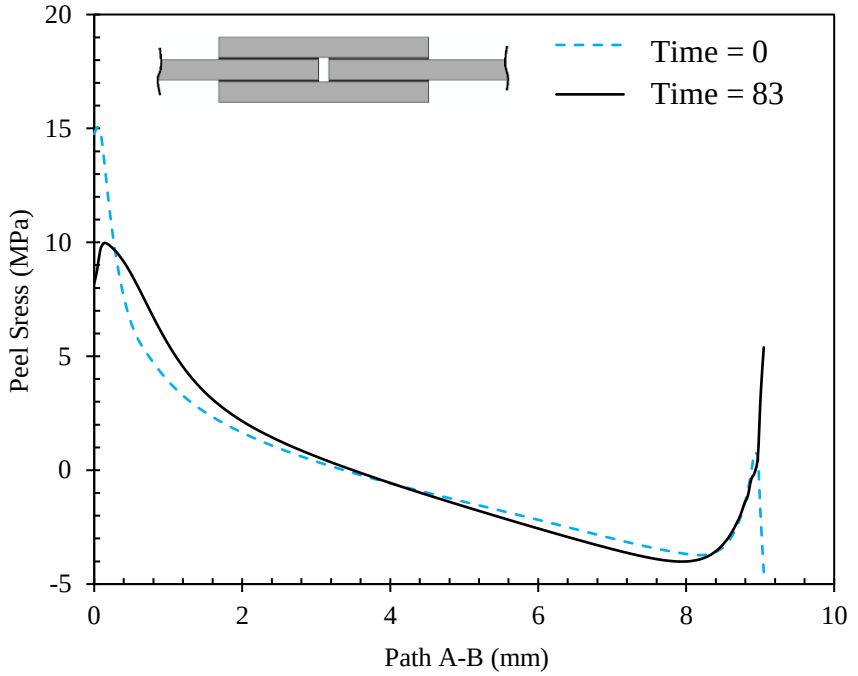
(f)

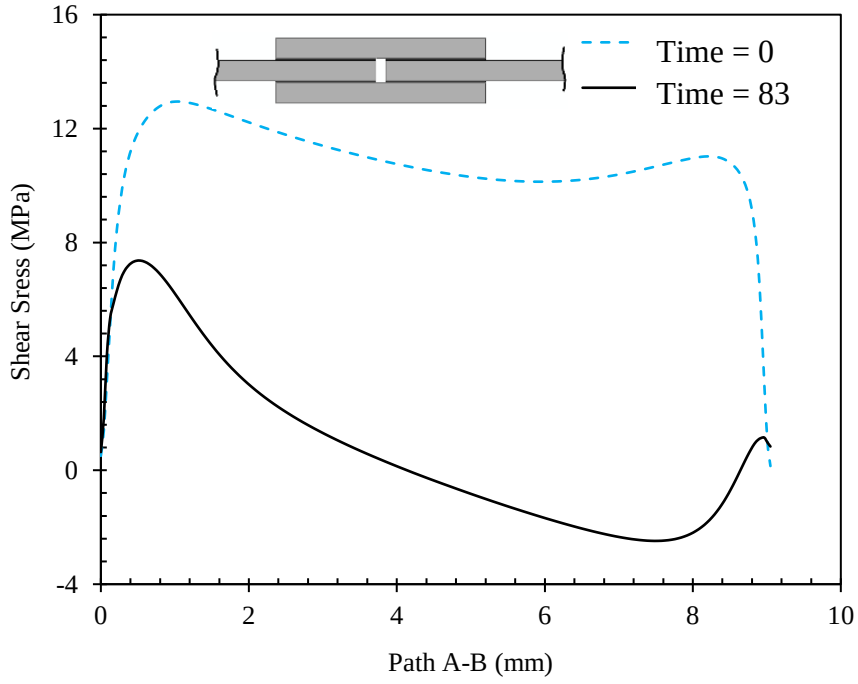
Fig. 10. Experimental and numerical time-elongation responses under creep loading of Single-Lap (SL) joints (a): l_a=19 mm (b): l_a=29 mm (c): l_a=39 mm and Double-Strap (DS) joints (d): l_a=19 mm (e): l_a=29 mm (f): l_a=39 mm.


Time = 0
Time = 83
Peel Sress (MPa)
Path A-B (mm)
16
12
8
4
0
-4
0
4
8
12
16
20


Time = 0
Time = 83
Shear Sress (MPa)
Path A-B (mm)
25
20
15
10
5
0
-5
0
4
8
12
16
20

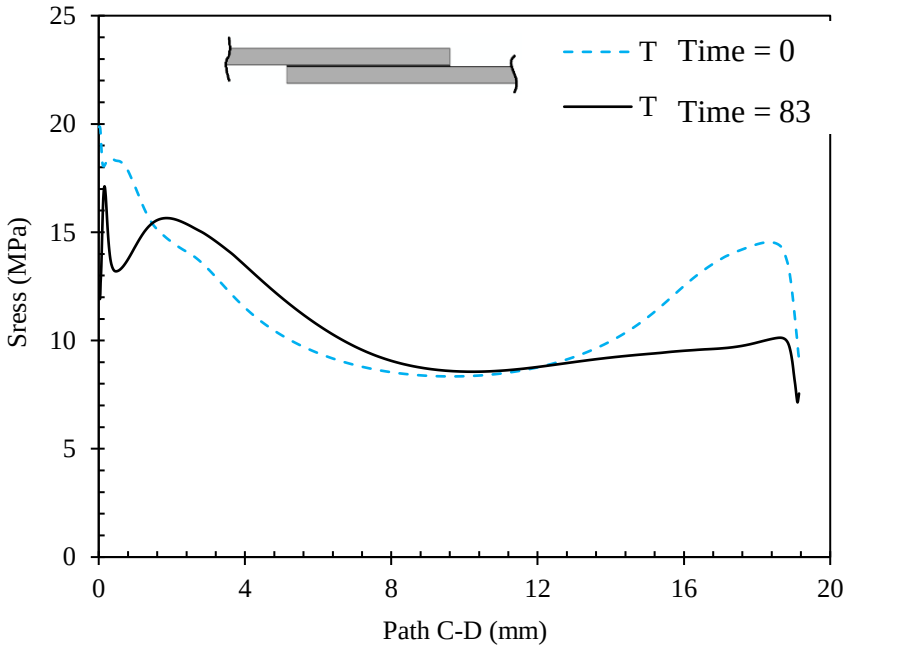
(a)



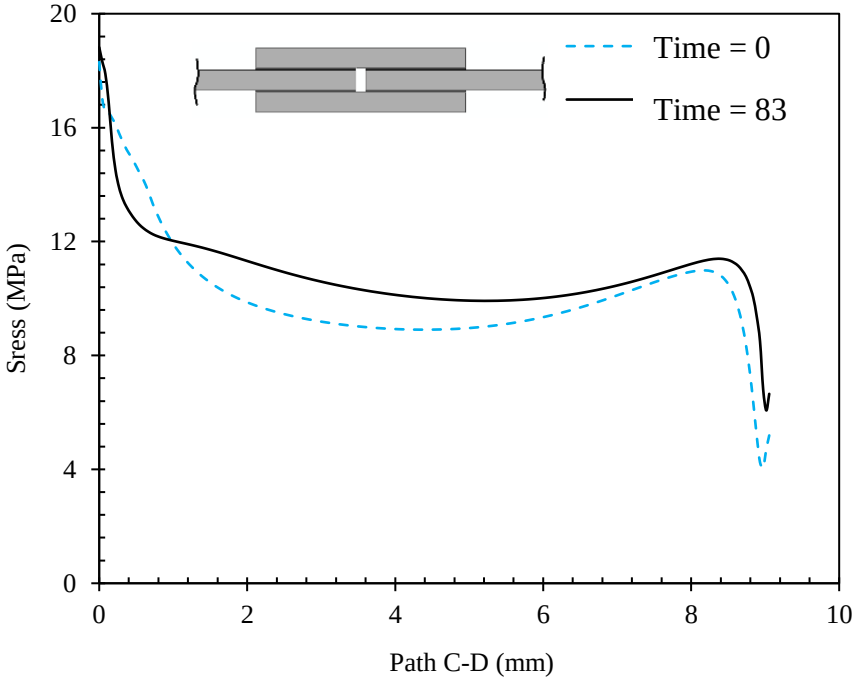


(b)

Fig. 11. Stress redistribution along the centre-line of the adhesive, path A-B. The result at the end of the loading step ($t \approx 0$) is given by a dashed line, while the result at the end of the creep test ($t \approx 83$ h) is given by a solid line. (a) Single-Lap (SL), and (b) Double-Strap (DS) joints.

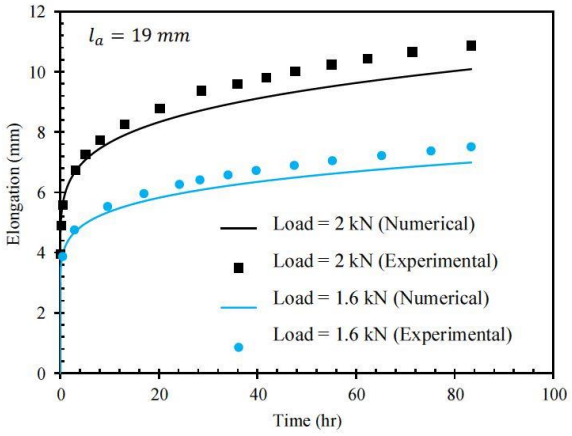


(a)

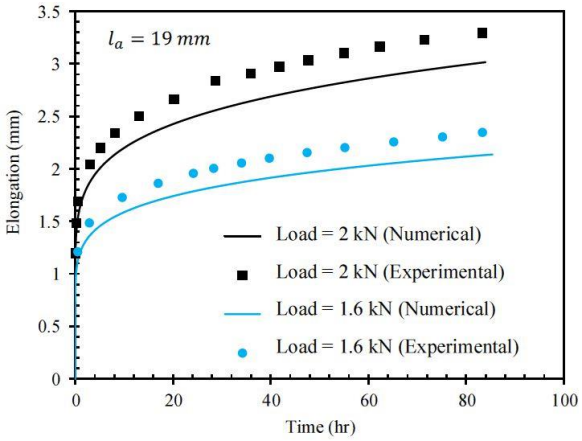


(b)

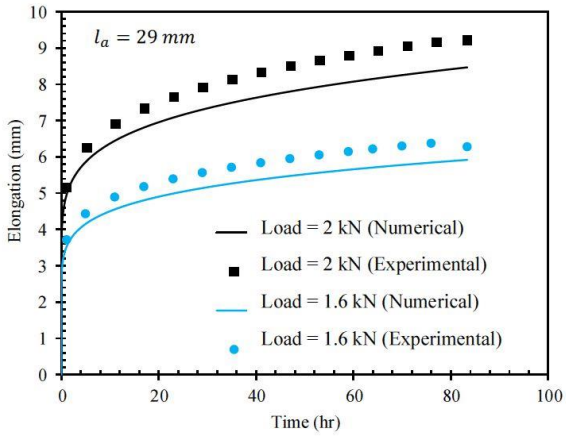
Fig.12 Stress redistribution along the centre-line of the adherent, path C-D. The result at the end of the loading step ($t \approx 0$) is given by a dashed line, while the result at the end of the creep test ($t \approx 83$ h) is given by a solid line. (a) Single-Lap (SL), and (b) Double-Strap (DS) joints


$l_a = 19\ mm$
Elongation (mm)
Time (hr)
Load = 2 kN (Numerical)
Load = 2 kN (Experimental)
Load = 1.6 kN (Numerical)
Load = 1.6 kN (Experimental)

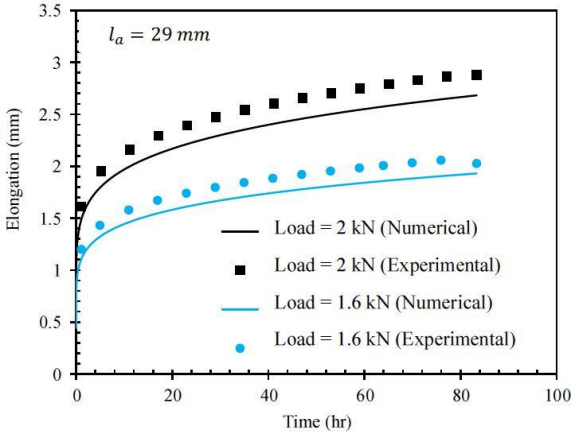
(a)


$l_a = 19\ mm$
Elongation (mm)
Time (hr)
Load = 2 kN (Numerical)
Load = 2 kN (Experimental)
Load = 1.6 kN (Numerical)
Load = 1.6 kN (Experimental)

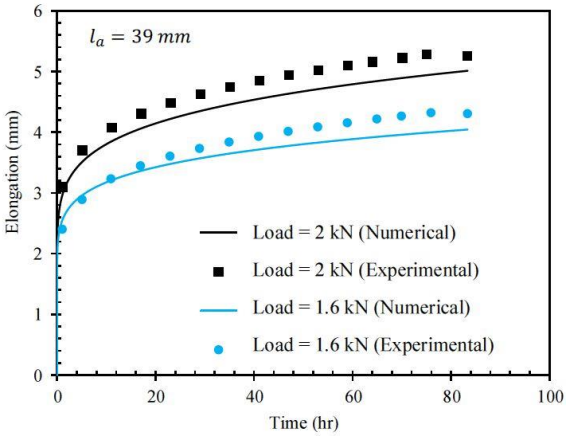
(d)


$l_a = 29\ mm$
Elongation (mm)
Time (hr)
Load = 2 kN (Numerical)
Load = 2 kN (Experimental)
Load = 1.6 kN (Numerical)
Load = 1.6 kN (Experimental)

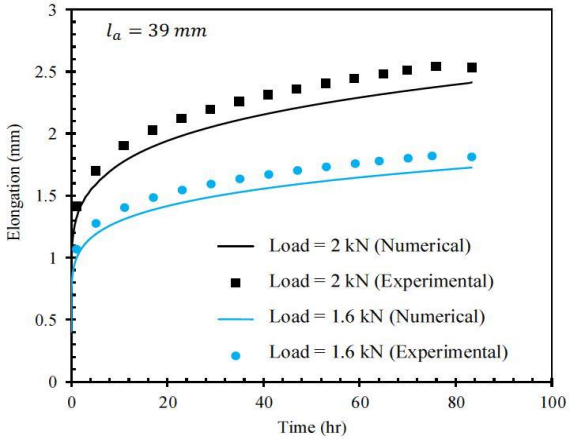
(b)


$l_a = 29\ mm$
Elongation (mm)
Time (hr)
Load = 2 kN (Numerical)
Load = 2 kN (Experimental)
Load = 1.6 kN (Numerical)
Load = 1.6 kN (Experimental)

(e)


$l_a = 39\ mm$
Elongation (mm)
Time (hr)
Load = 2 kN (Numerical)
Load = 2 kN (Experimental)
Load = 1.6 kN (Numerical)
Load = 1.6 kN (Experimental)

(c)


$l_a = 39\ mm$
Elongation (mm)
Time (hr)
Load = 2 kN (Numerical)
Load = 2 kN (Experimental)
Load = 1.6 kN (Numerical)
Load = 1.6 kN (Experimental)

(f)

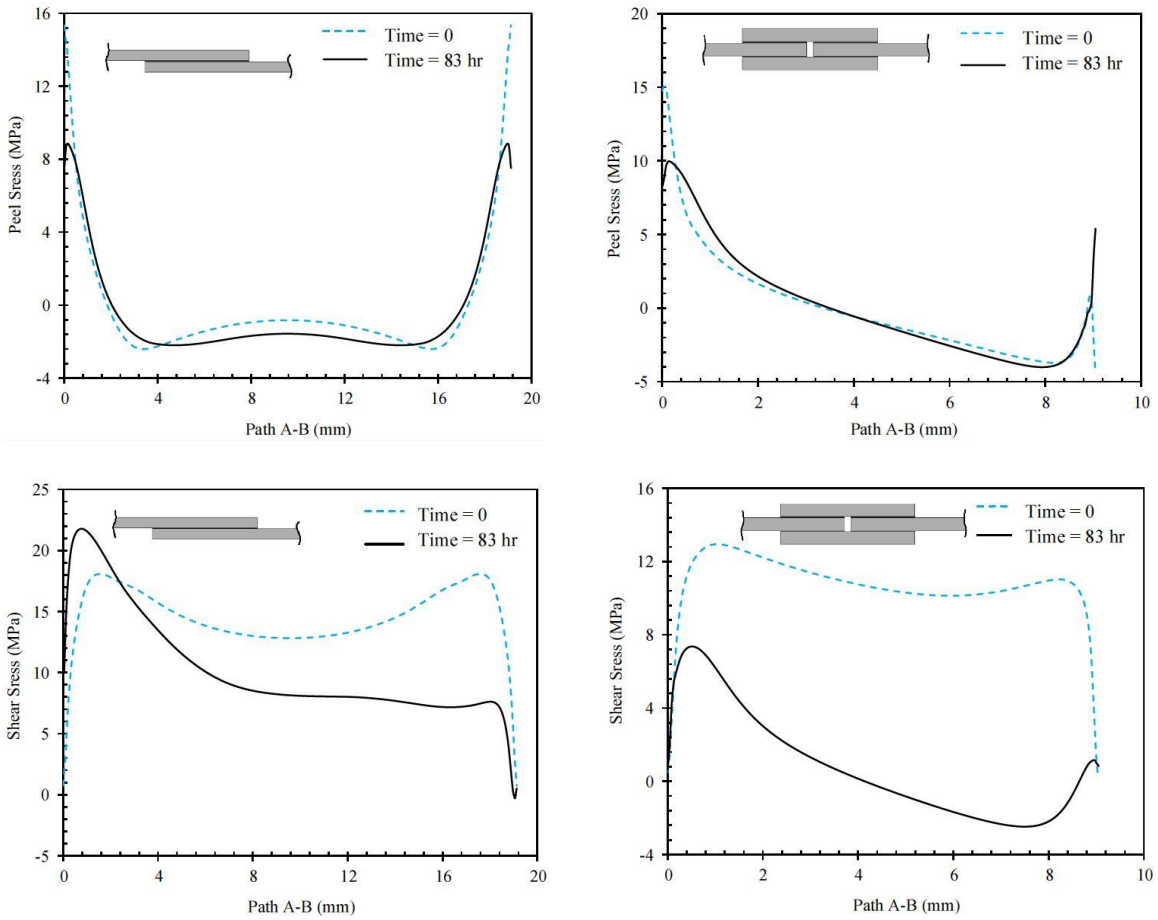


Fig.12 Stress redistribution along the centre-line of the adherent, path C-D. The result at the end of the loading step ($t \approx 0$) is given by a dashed line, while the result at the end of the creep test ($t \approx$ 83 h) is given by a solid line. (a) Single-Lap (SL), and (b) Double-Strap (DS) joints